IEEE Access
Multidisciplinary ⋮ Rapid Review ⋮ Open Access Journal

Received November 4, 2018, accepted November 17, 2018, date of publication November 29, 2018, date of current version December 27, 2018.

Digital Object Identifier 10.1109/ACCESS.2018.2884014

Performance Analysis of User Pairing in Cooperative NOMA Networks

JIAZHEN ZHANG, (Student Member, IEEE), XIAOFENG TAO, (Senior Member, IEEE), HUICI WU, (Member, IEEE) AND XUEFEI ZHANG, (Member, IEEE)

National Engineering Laboratory for Mobile Network Technologies, Beijing University of Posts and Telecommunications, Beijing 100876, China

Corresponding author: Xiaofeng Tao (taoxf@bupt.edu.cn)

This work was supported in part by the National Science and Technology Major Project under Grant 2018ZX03001029-004, in part by the National Natural Science Foundation for Distinguished Young Scholars of China under Grant 61325006, in part by the National Natural Science Foundation of China under Grant 61701037, and in part by the 111 Project of China under Grant B16006.

ABSTRACT In this paper, we study the coverage probability and average data rate of user pairing in cooperative non-orthogonal multiple access (NOMA) networks. With fixed locations of the source and typical user, the candidate users for pairing follow homogeneous Poisson point process. Considering the geometric distance between nodes, close-to-user pairing (CUP) and close-to-source pairing (CSP) schemes are investigated with the near user acting as half-duplex relay or full-duplex (FD) relay. Lower bounds on the coverage probability and average data rate are approximately obtained using stochastic geometry and Gaussian–Chebyshev quadrature. Numerical and simulation results corroborate the accuracy of the analytical results and reveal that CUP-based cooperative NOMA outperforms CSP-based cooperative NOMA in terms of the data rate performance. With typical user close to the source, CUP-based FD NOMA is the best transmission scheme (among CUP-based and CSP-based cooperative NOMA, non-cooperative NOMA, and OMA schemes) that maximizes the sum data rate and the minimum user rate.

INDEX TERMS Cooperative NOMA, user pairing, randomly deployed users, minimum user rate.

I. INTRODUCTION

With the densification of devices and the emergence of new applications, the ever-increasing demand for massive mobile access and high data traffic inspires the study of novel wireless access technologies [1]–[3]. Power-domain non-orthogonal multiple access (NOMA), a promising radio access technology, multiplexes multiple users on one resource block with superposition coding and power allocation. Successive interference cancelation (SIC) is applied at receivers for decoding. The advantages of NOMA in accommodating the ever dense users and approaching multiuser capacity region [4] benefit its application in Internet of things (IoT) and cellular networks.

In the conventional non-cooperative NOMA system, non-orthogonal users with different channel conditions experience huge performance difference and less user fairness. To improve the reliability of weak users with poor channel conditions, cooperative NOMA is studied to exploit the advantage of SIC at the strong user with good channel conditions by cooperatively forwarding the decoded signals to weak users. User pairing, the key in reducing the complexity and achieving the capacity gain of cooperative NOMA systems, has attracted great attentions [5]–[14].

A. MOTIVATION AND CONTRIBUTION

Most of the existing literatures on user pairing in cooperative NOMA networks assumed predesignated user pair and fixed user locations [5]–[12]. For a cooperative NOMA network with randomly deployed users, the source was located at the center of the cell and users were divided into near region users and far region users depending on their distances from source [13], [14]. A near region user and a far region user were selected as a user pair. The near one acted as relay to forward the signals of far user. This type of user pairing assures comparatively small distance between the source and near user, and the cooperative diversity cannot be fully exploited. In fact, when the distance between paired users is small, the performance of near user may degrade but the cooperative diversity of far user improves. However, in cooperative NOMA networks, the impact of the geometric distance between nodes on user pairing has not been fully explored yet.

In this paper, we investigate distance-based user pairing in the cooperative NOMA network, where the locations of the source and typical user are fixed, and the candidate users for pairing follow the distribution of homogeneous Poisson Point Process (PPP) [15].

Firstly, Close-to-User Pairing (CUP) scheme and Close-to-Source Pairing (CSP) scheme are presented, where the candidate user closest to the typical user and source within the pairing region is chosen as the pairing user of typical user respectively. For the typical user and pairing user, we define the near user as the one nearer to the source, and accordingly the other one is the far user. The near user employs SIC and cooperatively forwards the signal of far user in either half-duplex (HD) NOMA or full-duplex (FD) NOMA mode.

Then, to evaluate the performance of the cooperative NOMA system, closed-form expressions for the lower bound on coverage probability and average data rate are approximately obtained with stochastic geometry and Gaussian-Chebyshev quadrature. Theoretical insights are also provided to explore the impact of the power allocation coefficient.

Finally, we define the best transmission scheme (among CUP-based and CSP-based cooperative NOMA, CSP-based non-cooperative NOMA, CUP-based and CSP-based orthogonal multiple access (OMA)) as the transmission scheme that achieves the maximum data rate performance. Numerical results validate the theoretical analysis and reveal that with optimal power allocation employed, CUP-based FD NOMA and CSP-based non-cooperative NOMA are the best transmission schemes that maximize the sum data rate and the minimum user rate with typical user close to and far from the source, respectively.

B. RELATED WORKS

The impact of user pairing in non-cooperative NOMA networks has been extensively studied in [16]–[21]. Ding *et al.* [16] performed two-user pairing and revealed that user pairs with larger difference in channel conditions achieved higher gain on sum rate over OMA. Considering non-uniform user distribution in a cell, a part of far users cannot be paired. To tackle this issue, virtual and time sharing-based user pairing schemes were proposed in [17] and [22] to realize one near user-multiple far users pairing. The effect of user pairing and power allocation on the bit error rate was studied in [18]. To improve the performance of the whole network, matching algorithm-based user pairing was developed in [19]. Researches on user pairing were also extended to multi-antenna and multi-cell scenarios in [20] and [21].

Most existing literatures on user pairing in cooperative NOMA networks considered predesignated user partition [5]–[12]. With fixed user locations, Yue *et al.* [5], [6] and Zhang *et al.* [7], [8] derived the outage probability and ergodic sum rate in HD NOMA and FD NOMA systems. Zhou *et al.* [13] and Liu *et al.* [14] considered a cell with the source located at the center, and randomly deployed candidate users were divided into near region users and far region users depending on their distances from source. A near region user and a far region user were selected as a user pair. The impact of the distance between paired users is neglected in the design of user pairing. On the other hand, Zhang *et al.* [8], Li *et al.* [9], and Liu *et al.* [10] aimed to minimize outage probability and power consumption of a user pair with power allocation. To reduce the difference in the data rate of paired users, the improvement of the minimum user rate should also be concerned about. Zhang *et al.* [8] and Liu *et al.* [12] maximized the minimum user rate of a user pair with power allocation. Do *et al.* [11] improved the performance of cell-edge users using on-off cooperative relaying schemes based on channel conditions of the direct and relaying links. The impact of user pairing and transmission mode (e.g., HD NOMA, FD NOMA, non-cooperative NOMA, OMA) on the data rate performance has not been fully studied.

C. ORGANIZATION

The remainder of this paper is organized as follows. In Section II, the system model as well as the received signal-to-interference-plus-noise ratios (SINRs) of CUP and CSP schemes are presented. In Section III and IV, the coverage probability and average data rate of the user pair are approximated. The simulation results are shown in Section V. Finally, this paper is summarized in Section VI.

II. SYSTEM MODEL

As illustrated in Fig. 1, we consider the downlink transmission in a cooperative NOMA network, where a source ($\mathcal{S}$) communications with a typical user ($\mathcal{U}_1$) and a pairing user of $\mathcal{U}_1$. The pairing user is selected among multiple candidate pairing users. Polar coordinate is employed. $\mathcal{S}$ is located at the origin $(0, 0)$. $\mathcal{U}_1$ is located at $(d_1, 0)$. The region for pairing is defined as a sector with maximum angle $\theta_0 = \pi$ and no constraint on the maximum distance. Within the pairing region, the candidate users are spatially distributed as homogeneous PPP Φ_u with density λ_u [15].

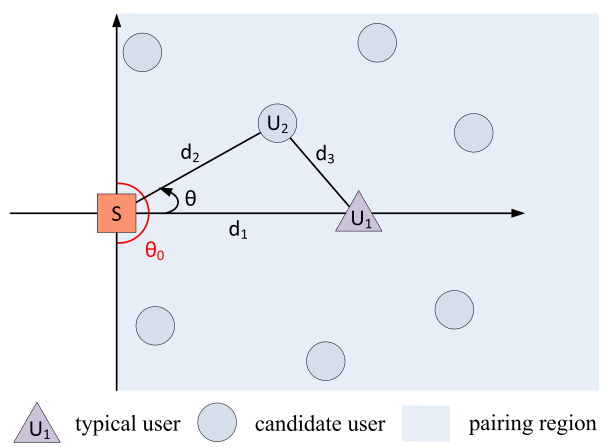

FIGURE 1. An illustration of downlink transmission in a cooperative NOMA network with a source node (red square), a typical user (purple triangle) and multiple candidate users (blue circles). The pairing region (blue shadow) is a sector with maximum angle $\theta_0 = \pi$ and no constraint on the maximum distance. Within the pairing region, the spatial distribution of the candidate users follows homogeneous PPP.

A. CUP AND CSP SCHEMES

With CUP (CSP) scheme, the candidate user closest to $\mathcal{U}_1$ ($\mathcal{S}$) within the pairing region is chosen as the pairing user of $\mathcal{U}_1$. Denote $\mathcal{U}_2$ as the pairing user of $\mathcal{U}_1$. Denote d_1, d_2, d_3 as the distance of the $\mathcal{S}$-$\mathcal{U}_1$, $\mathcal{S}$-$\mathcal{U}_2$, $\mathcal{U}_1$-$\mathcal{U}_2$ links, respectively. $\mathcal{U}_2$ is located at (d_2, θ), where $\theta = \angle \mathcal{U}_2 \mathcal{S} \mathcal{U}_1 \in [-\frac{\pi}{2}, \frac{\pi}{2}]$ is the rotation.

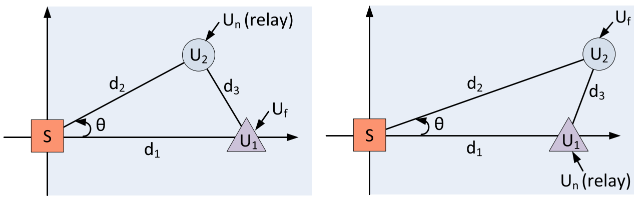

(a) (b)

FIGURE 2. An illustration of CUP scheme, where $\mathcal{U}_1$ is the typical user, $\mathcal{U}_2$ is the pairing user of $\mathcal{U}_1$.

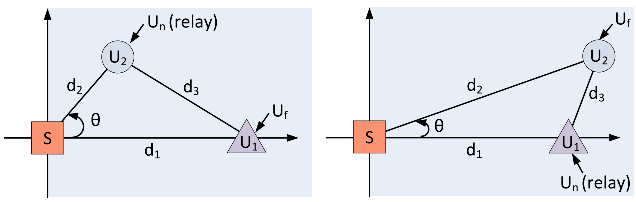

(a) (b)

FIGURE 3. An illustration of CSP scheme, where $\mathcal{U}_1$ is the typical user, $\mathcal{U}_2$ is the pairing user of $\mathcal{U}_1$.

$\mathcal{S}$ serves the user pair with power-domain NOMA. As shown in Fig. 2 and Fig. 3, we define the near user $\mathcal{U}_n$ as the user nearer to $\mathcal{S}$, and the other one is the far user $\mathcal{U}_f$. For example, in Fig. 2(a), $d_1 \geq d_2$, thus $\mathcal{U}_n = \mathcal{U}_2, \mathcal{U}_f = \mathcal{U}_1$. In Fig. 2(b), $d_1 < d_2$, thus $\mathcal{U}_n = \mathcal{U}_1, \mathcal{U}_f = \mathcal{U}_2$. The near user acts as a decode-and-forward (DF) relay, which decodes the signal of far user and its own by employing SIC [23] and forwards the signal of far user in either HD NOMA or FD NOMA mode.[1] $\mathcal{S}$ is equipped with single antenna. To enable FD communication, the users are equipped with one transmit antenna and one receive antenna.

B. RADIO PROPAGATION MODEL AND RECEIVED SINR

Radio signals undergo both standard path loss propagation and flat block Rayleigh fading. Denote $\bar{h}_1$, $\bar{h}_2$, $\bar{h}_3$ as the complex channel coefficient of the $\mathcal{S}$-$\mathcal{U}_1$, $\mathcal{S}$-$\mathcal{U}_2$ and $\mathcal{U}_n$-$\mathcal{U}_f$ links, respectively. $h_i = |\bar{h}_i|^2 (i \in \{1, 2, 3\})$ is the Rayleigh fading gain, which is exponential distributed with unit mean. Denote I_n, I_f as the inter-user interference from non-serving sources experienced at $\mathcal{U}_n$, $\mathcal{U}_f$ respectively. I_n, I_f can be regarded as noise with constant power I_{inter} since the statistic of interference obeys a stationary distribution when users follow the PPP model [26]. Denote n_n, n_f as the additive white Gaussian noise (AWGN) at $\mathcal{U}_n, \mathcal{U}_f$ respectively, and the average noise power is σ_0^2.

[1] Differently from the incremental relaying networks where the relaying user only serves as a helper of the destination based on channel states [24], [25], the focal point of the cooperative NOMA is the data rate of both paired users.

1) HD NOMA

When $\mathcal{U}_n$ operates in the HD NOMA mode, the transmission is partitioned into two phases. Each phase lasts one time slot. In the first phase (i.e., odd time slot), $\mathcal{S}$ transmits the superposed signal of $\mathcal{U}_n$ and $\mathcal{U}_f$, i.e.,

$$y_a[2k-1] = \sqrt{a_n P_a} x_n[2k-1] + \sqrt{a_f P_a} x_f[2k-1], \quad (1)$$

where $2k-1$ is the time index, $k = 1, 2, 3, \ldots$, P_a is the transmit power of $\mathcal{S}$, x_n and x_f are the signals for $\mathcal{U}_n$ and $\mathcal{U}_f$ respectively, $E\left[|x_1|^2\right] = E\left[|x_2|^2\right] = 1$. a_n and a_f are the power allocation coefficients for x_n and x_f respectively, $a_n + a_f = 1$. SIC is adopted at $\mathcal{U}_n$ and the signal of $\mathcal{U}_f$ is firstly decoded by treating the signal of $\mathcal{U}_n$ as interference. The received SINR at $\mathcal{U}_n$ to detect $x_f[2k-1]$, defined as $\gamma_{n,f}^{\mathrm{H}}$, is given as

$$\gamma_{n,f}^{\mathrm{H}} = \frac{a_f P_a h_n d_n^{-\alpha}}{a_n P_a h_n d_n^{-\alpha} + \sigma^2}, \quad (2)$$

where $\sigma^2 = I_{\text{inter}} + \sigma_0^2$ is a constant. After $\mathcal{U}_n$ successfully decodes $x_f[2k-1]$, it removes $x_f[2k-1]$ from the received signal and decodes its own signal. The received SINR of $x_n[2k-1]$ at $\mathcal{U}_n$ is

$$\gamma_{n,n}^{\mathrm{H}} = \frac{a_n P_a h_n d_n^{-\alpha}}{\sigma^2}. \quad (3)$$

The received SINR at $\mathcal{U}_f$ to detect $x_f[2k-1]$ for direct link is $\frac{a_f P_a h_f d_f^{-\alpha}}{a_n P_a h_f d_f^{-\alpha} + \sigma^2}$.

In the second phase (i.e., even time slot), $\mathcal{U}_n$ cooperatively forwards the decoded signal $x_f[2k]$ to $\mathcal{U}_f$. The SINR at $\mathcal{U}_f$ to detect $x_f[2k]$ for relaying link (the $\mathcal{U}_n$-$\mathcal{U}_f$ link) is $\frac{P_u h_3 d_3^{-\alpha}}{\sigma^2}$, where P_u is the transmit power of $\mathcal{U}_n$. $\mathcal{U}_f$ combines the signals from the relaying link and direct link by maximal ratio combining (MRC) [23]. The received SINR after MRC at $\mathcal{U}_f$ is

$$\gamma_{f,f}^{\mathrm{H}} = \frac{a_f P_a h_f d_f^{-\alpha}}{a_n P_a h_f d_f^{-\alpha} + \sigma^2} + \frac{P_u h_3 d_3^{-\alpha}}{\sigma^2}. \quad (4)$$

2) FD NOMA

When $\mathcal{U}_n$ operates in the FD NOMA mode, the direct and cooperative transmissions are executed at the same frequency band simultaneously. In the k-th time slot, $\mathcal{S}$ transmits the superposed signal $y_a[k] = \sqrt{a_n P_a} x_n[k] + \sqrt{a_f P_a} x_f[k]$, meanwhile $\mathcal{U}_n$ tends to decode signal $x_f[k]$ and forward $x_f[k]$ to $\mathcal{U}_f$. When $\mathcal{U}_n$ employs SIC technique, the receiver at $\mathcal{U}_n$ also suffers from residual self-interference from its transmit antenna to its receive antenna. An imperfect self-interference cancelation scheme is performed at $\mathcal{U}_n$ as in [6]. The self-interference cancelation factor is denoted as κ $(0 \leq \kappa \leq 1)$, which demonstrates the degree of self-interference cancelation. The $\mathcal{U}_n$-$\mathcal{U}_n$ link does not experience path loss, instead it is modeled as a Rayleigh fading channel with coefficient $\bar{h}_u$. $h_u = |\bar{h}_u|^2$ is exponential distributed with average power μ.

Based on the radio propagation model, the observation at $\mathcal{U}_n$ is $y_n[k] = \bar{h}_n[k]y_a[k] + \sqrt{\kappa P_u}\bar{h}_u[k]s[k] + I_n[k] + n_n[k]$, where $s[k]$ is the transmit signal of $\mathcal{U}_n$. By employing SIC, the received SINR of $x_f[k]$ at $\mathcal{U}_n$ is

$$\gamma_{n,f}^{\mathrm{F}} = \frac{a_f P_a h_n d_n^{-\alpha}}{a_n P_a h_n d_n^{-\alpha} + \kappa P_u h_u + \sigma^2}. \tag{5}$$

When $\mathcal{U}_n$ can successfully decode $x_f[k]$, $s[k] = x_f[k - k_d]$, where k_d is the processing delay at $\mathcal{U}_n$ (We assume $k_d = 1$ and $k_d \leq k$ here.) [8]. After $\mathcal{U}_n$ removes $x_f[k]$ from the received signal $y_n[k]$, the received SINR of $x_n[k]$ at $\mathcal{U}_n$ is

$$\gamma_{n,n}^{\mathrm{F}} = \frac{a_n P_a h_n d_n^{-\alpha}}{\kappa P_u h_u + \sigma^2}. \tag{6}$$

The received signal at $\mathcal{U}_f$ is $y_f[k] = \bar{h}_f[k]y_a[k] + \sqrt{P_u}\bar{h}_3[k]x_f[k - k_d] + I_f[k] + n_f[k]$. There exists small time delay between the signals from $\mathcal{S}$ and $\mathcal{U}_n$. As in [6]–[8], we assume that the two signals from $\mathcal{S}$ and $\mathcal{U}_n$ are fully resolvable at $\mathcal{U}_f$, and they can be appropriately cophased and merged by MRC. Consequently, the received SINR after MRC at $\mathcal{U}_f$ is the same as that in the HD NOMA case, i.e., $\gamma_{f,f}^{\mathrm{F}} = \gamma_{f,f}^{\mathrm{H}}$.

Remark 1: In 5G scenarios, the base station (BS) is equipped with massive antennas, but only partial antennas at BS are selected to serve a user pair [27]–[29]. Yu *et al.* [29] assumed that the BS selects one out of N available antennas to serve one user pair, so that the hardware cost and complexity at BS can be reduced and only partial channel state information (CSI) is required.

With multiple antennas serving a user pair, the performance analysis can also be performed based on the analytical framework in this paper. Assuming that $\mathcal{S}$ is equipped with M_T antennas, and L_T ($L_T < M_T$) antennas at $\mathcal{S}$ are selected to communicate with the user pair. The channel vectors from $\mathcal{S}$ to near user and far user are defined as $H_n = [\bar{h}_{1,n}, \bar{h}_{2,n}, \ldots, \bar{h}_{L_T,n}]$ and $H_f = [\bar{h}_{1,f}, \bar{h}_{2,f}, \ldots, \bar{h}_{L_T,f}]$, respectively, where $\bar{h}_{k,n}$ ($\bar{h}_{k,f}$), $k = 1, 2, \ldots, L_T$, is the channel coefficient between the k-th selected antenna of $\mathcal{S}$ and near user (far user). The channels between $\mathcal{S}$ and users undergo flat block Rayleigh fading. $h_{k,n} = |\bar{h}_{k,n}|^2$ and $h_{k,f} = |\bar{h}_{k,f}|^2$ are the Rayleigh fading gains, which are exponential distributed with unit mean. Since the channel gains are vectors, it is challenging to design antenna selection and the decoding order of SIC. Multi-antenna system can further improve the performance of the NOMA system, however, it is beyond the scope of this paper and will be studied in our future work.

In the following sections, we evaluate the coverage and data rate performance of paired users with CUP and CSP schemes, and further study the impact of user pairing, transmission mode and power allocation on the system performance. In the rest of this paper, we will drop the time index for brevity.

III. COVERAGE PROBABILITY

In this section, the coverage probability of the cooperative NOMA system is analyzed with stochastic geometry and Gaussian-Chebyshev quadrature [30].

Define τ_1, τ_2 as the SINR thresholds of decoding x_1 and x_2 respectively. $\mathcal{U}_n$ is in coverage when it can successfully decode both the signal of $\mathcal{U}_f$ and its own. $\mathcal{U}_f$ is in coverage in two cases: 1) $\mathcal{U}_n$ can decode signal x_f and the received SINR after MRC at $\mathcal{U}_f$ is larger than τ_f; 2) $\mathcal{U}_n$ cannot decode signal x_f and the received SINR for direct link at $\mathcal{U}_f$ is larger than τ_f. For Case 2, when $\mathcal{U}_n$ fails to decode x_f, it is more difficult to decode x_f at $\mathcal{U}_f$ due to the severe path loss of $\mathcal{S}$-$\mathcal{U}_f$ link. Thus, we mostly study Case 1 in this paper for simplification.

A. CUP SCHEME

With CUP scheme, we transform the origin to $\mathcal{U}_1$. As shown in Fig. 4, $\mathcal{U}_1$ is located at $(0, 0)$. $\mathcal{S}$ is located at (d_1, π). Denote (r, θ) as the polar coordinate of $\mathcal{U}_2$. $r = d_3$, $\theta = \angle \mathcal{U}_2\mathcal{U}_1 x \in (0, 2\pi]$ is the rotation. Before evaluating coverage performance, we firstly give out the probability of $d_1 > d_2$.

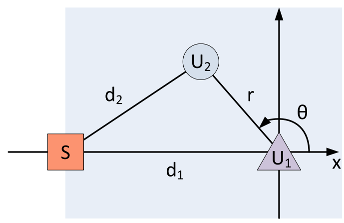

FIGURE 4. The polar coordinate for CUP scheme.

Lemma 1: With CUP scheme, the probability that $\mathcal{U}_1$ serves as far user is

$$\begin{aligned}
&\mathcal{P}_{1\to\mathrm{far}}^{\mathrm{CUP}} \\
&\approx \frac{1}{N}\sum_{n=1}^{N}\sin\left(\frac{2n-1}{2N}\pi\right)\frac{1-e^{-\frac{\pi\lambda_u\phi_1^2}{2}}}{\sqrt{8-\left(\frac{\phi_1}{d_1}\right)^2}} \\
&\quad + \frac{1}{M}\sum_{m=1}^{M}\sin\left(\frac{2m-1}{2M}\pi\right)\frac{\left(2-\sqrt{2}\right)\left(1-e^{-\frac{16\pi\lambda_u d_1^2}{(\phi_2+2\sqrt{2})^2}}\right)}{\sqrt{16-(\phi_2+2\sqrt{2})^2}},
\end{aligned} \tag{7}$$

where $\phi_1 = \left(1+\cos\left(\frac{2n-1}{2N}\pi\right)\right)d_1$, $\phi_2 = \left(1+\cos\left(\frac{2m-1}{2M}\pi\right)\right)\left(2-\sqrt{2}\right)$, N, M are parameters to ensure accuracy at the cost of certain computational complexity.

Proof: Please refer to Appendix A. ■

1) HD NOMA

In this subsection, we characterize the coverage probability of the user pair in HD NOMA networks.

Theorem 1: With CUP-based HD NOMA, when $\mathcal{U}_1$ is the far user, the coverage probability of $\mathcal{U}_2$ is approximated as

$$\begin{aligned}
&\mathcal{P}_{2\to \text{near}}^{\text{HD-CUP}} \\
&\approx \mathbf{1}(a_f > \frac{\tau_1}{1+\tau_1})\frac{2\pi^2}{MN}\sum_{m=1}^{M}\sum_{n=1}^{N} \\
&\quad\times \sin\left(\frac{2m-1}{2M}\pi\right)\sin\left(\frac{2n-1}{2N}\pi\right) \\
&\quad\times \left[\Xi_{2\to \text{near}}^{\text{HD-CUP,covI}} \frac{\lambda_u \phi_1 \phi_3^2 d_1 e^{-\frac{\pi\lambda_u \phi_1^2\phi_3^2}{2}}}{4\sqrt{2-\phi_3{}^2}} \right. \\
&\quad\left. +\ \Xi_{2\to \text{near}}^{\text{HD-CUP,covII}} \frac{4(2-\sqrt{2})\lambda_u d_1 \phi_1 e^{-\frac{4\pi\lambda_u d_1^2}{(\phi_2+2\sqrt{2})^2}}}{\left((\phi_2+2\sqrt{2})^2\right)\sqrt{16-(\phi_2+2\sqrt{2})^2}} \right],
\end{aligned} \tag{8}$$

where

$$\begin{aligned}
\Xi_{2\to \text{near}}^{\text{HD-CUP,covI}} &= \frac{e^{-A\omega_1}}{\mathcal{P}_{1\to \text{far}}^{\text{CUP}}}, \\
\Xi_{2\to \text{near}}^{\text{HD-CUP,covII}} &= \frac{e^{-A\omega_2}}{\mathcal{P}_{1\to \text{far}}^{\text{CUP}}}, \\
A &= \begin{cases} \dfrac{\sigma^2\tau_1}{P_a\left(a_f-a_n\tau_1\right)} & \tau_2 \le B,\ a_f > \dfrac{\tau_1}{1+\tau_1} \\ \dfrac{\sigma^2\tau_2}{a_n P_a} & \tau_2 > B,\ a_f > \dfrac{\tau_1}{1+\tau_1}, \end{cases} \\
B &= \frac{a_n\tau_1}{1-a_n\left(1+\tau_1\right)}, \\
\omega_1 &= \left(\frac{\phi_1^2\phi_3^2}{2}+d_1^2-\phi_1\phi_3^2 d_1\right)^{\frac{\alpha}{2}}, \\
\omega_2 &= \left(\frac{4\phi_1^2}{(\phi_2+2\sqrt{2})^2}+d_1^2-\phi_1 d_1\right)^{\frac{\alpha}{2}}, \\
\phi_3 &= \frac{1+\cos\left(\frac{2m-1}{2M}\pi\right)}{2}.
\end{aligned}$$

The lower bound on the coverage probability of $\mathcal{U}_1$ is approximated as

$$\begin{aligned}
&\underline{\mathcal{P}}_{1\to \text{far}}^{\text{HD-CUP}} \\
&\approx \mathbf{1}(a_f > \frac{\tau_1}{1+\tau_1})\frac{2\pi^2}{MN}\sum_{m=1}^{M}\sum_{n=1}^{N} \\
&\quad\times \sin\left(\frac{2m-1}{2M}\pi\right)\sin\left(\frac{2n-1}{2N}\pi\right) \\
&\quad\times \left[\Xi_{1\to \text{far}}^{\text{HD-CUP,covI}} \frac{\lambda_u \phi_1 \phi_3^2 d_1 e^{-\frac{\pi\lambda_u \phi_1^2\phi_3^2}{2}}}{4\sqrt{2-\phi_3{}^2}} \right. \\
&\quad\times \left(1+E\left(\frac{\phi_1\phi_3}{\sqrt{2}}\right)^{\alpha}\left(2c_0+\ln\left(E\left(\frac{\phi_1\phi_3}{\sqrt{2}}\right)^{\alpha}\right)\right)\right) \\
&\quad +\ \Xi_{1\to \text{far}}^{\text{HD-CUP,covII}} \frac{4(2-\sqrt{2})\lambda_u d_1 \phi_1 e^{-\frac{4\pi\lambda_u d_1^2}{(\phi_2+2\sqrt{2})^2}}}{\left((\phi_2+2\sqrt{2})^2\right)\sqrt{16-(\phi_2+2\sqrt{2})^2}} \\
&\quad\left. \times \left(1+E\left(\frac{2\phi_1}{\phi_2+2\sqrt{2}}\right)^{\alpha}\left(2c_0+\ln\left(E\left(\frac{2\phi_1}{\phi_2+2\sqrt{2}}\right)^{\alpha}\right)\right)\right)\right],
\end{aligned} \tag{11}$$

where

$$\begin{aligned}
\Xi_{1\to \text{far}}^{\text{HD-CUP,covI}} &= \frac{e^{-C\omega_1-D\left(\frac{\phi_1\phi_3}{\sqrt{2}}\right)^{\alpha}}}{\mathcal{P}_{1\to \text{far}}^{\text{CUP}}}, \\
\Xi_{1\to \text{far}}^{\text{HD-CUP,covII}} &= \frac{e^{-C\omega_2-D\left(\frac{2\phi_1}{\phi_2+2\sqrt{2}}\right)^{\alpha}}}{\mathcal{P}_{1\to \text{far}}^{\text{CUP}}}, \\
C &= \frac{\sigma^2\tau_1}{P_a\left(a_f-a_n\tau_1\right)}, \quad D = \frac{\sigma^2}{P_u}\left(\tau_1-\frac{a_f}{a_n}\right), \\
E &= \frac{\sigma^4 a_f d_1^{\alpha}}{a_n^2 P_u P_a}, \quad c_0 = -\frac{\varphi(1)}{2}-\frac{\varphi(2)}{2},
\end{aligned}$$

and $\varphi(\cdot)$ denotes the psi function [31].

Proof: Please refer to Appendix B. ■

Remark 2: When $\mathcal{U}_1$ is the far user, $a_f \in (\frac{\tau_1}{1+\tau_1}, 1]$ in (8) assures non-negative $\gamma_{2,1}^{\text{H}} - \tau_1$. If this condition is violated, outage event occurs at the near user.

With low transmit signal-to-noise ratio (SNR) $\frac{P_a}{\sigma^2}$, when $a_f \in \left(\frac{\tau_1}{1+\tau_1}, \frac{\tau_1(1+\tau_2)}{\tau_1+\tau_2+\tau_1\tau_2}\right]$, $A = \frac{\sigma^2\tau_1}{P_a(a_f-a_n\tau_1)}$ and $\mathcal{P}_{2\to \text{near}}^{\text{HD-CUP}}$ increases with a_f. In this scenario, the bottleneck of performance improvement is the decoding of x_f at the near user, thus the coverage is improved when more power is allocated to signal x_f. When $a_f \in \left(\frac{\tau_1(1+\tau_2)}{\tau_1+\tau_2+\tau_1\tau_2}, 1\right)$, $A = \frac{\sigma^2\tau_2}{a_n P_a}$ and $\mathcal{P}_{2\to \text{near}}^{\text{HD-CUP}}$ decreases with a_f. The bottleneck of performance improvement is the decoding of x_n, thus the coverage becomes worse when less power is remained for x_n. Based on (9), $\underline{\mathcal{P}}_{1\to \text{far}}^{\text{HD-CUP}}$ increases with growing a_f since the increase of a_f enhances $\gamma_{2,1}^{\text{H}}$ and $\gamma_{1,1}^{\text{H}}$.

Theorem 2: With CUP-based HD NOMA, when $\mathcal{U}_1$ is the near user, the coverage probability of $\mathcal{U}_1$ is

$$\mathcal{P}_{1\to \text{near}}^{\text{HD-CUP}} = \mathbf{1}(a_f > \frac{\tau_2}{1+\tau_2})e^{-F}, \tag{10}$$

where

$$\begin{aligned}
F &= \begin{cases} \dfrac{\sigma^2\tau_2 d_1^{\alpha}}{P_a\left(a_f-a_n\tau_2\right)} & \tau_1 \le G, a_f > \dfrac{\tau_2}{1+\tau_2} \\ \dfrac{\sigma^2\tau_1 d_1^{\alpha}}{a_n P_a}\tau_1 > G, & a_f > \dfrac{\tau_2}{1+\tau_2} \end{cases}, \\
G &= \frac{a_n\tau_2}{1-a_n\left(1+\tau_2\right)}.
\end{aligned}$$

The lower bound on the coverage probability of $\mathcal{U}_2$ is

$$\underline{\mathcal{P}}_{2\to \text{far}}^{\text{HD-CUP}} \approx \mathbf{1}(a_f > \frac{\tau_2}{1+\tau_2})\left(\varphi_1+\varphi_2+\varphi_3\right), \tag{11}$$

where $\varphi_1, \varphi_2, \varphi_3$ are given in (12)-(14), as shown at the top of the next page, $\Xi_{2\to \text{far}}^{\text{HD-CUP,cov}} = \left\{ \frac{e^{-J-K\omega_3^{\alpha}}}{1-\mathcal{P}_{1\to \text{far}}^{\text{CUP}}}, \frac{e^{-J-K\phi_4^{\alpha}}}{1-\mathcal{P}_{1\to \text{far}}^{\text{CUP}}}, \right.$

$$\varphi_1 \approx \frac{2\pi^2}{MN}\sum_{m=1}^{M}\sum_{n=1}^{N}\sin\left(\frac{2m-1}{2M}\pi\right)\sin\left(\frac{2n-1}{2N}\pi\right)\Xi_{2\to\mathrm{far}}^{\mathrm{HD-CUP,cov}}\lambda_u\omega_3 e^{-\pi\lambda_u\omega_3^2}\frac{\sqrt{2}d_1(1-\phi_3^2)}{4\phi_3\sqrt{2-{\phi_3}^2}}$$
$$\times\left(1+L\omega_3^{\alpha}(d_1^2+\omega_3^2-\sqrt{2}\omega_3 d_1\phi_3)^{\frac{\alpha}{2}}\left(\ln\left(L\omega_3^{\alpha}(d_1^2+\omega_3^2-\sqrt{2}\omega_3 d_1\phi_3)^{\frac{\alpha}{2}}\right)+2c_0\right)\right) \tag{12}$$

$$\varphi_2 \approx \frac{\pi^2}{2MN}\sum_{m=1}^{M}\sum_{n=1}^{N}\sin\left(\frac{2m-1}{2M}\pi\right)\sin\left(\frac{2n-1}{2N}\pi\right)\Xi_{2\to\mathrm{far}}^{\mathrm{HD-CUP,cov}}\lambda_u\phi_4 e^{-\pi\lambda_u\phi_4^2}\frac{1}{\sqrt{1-{\phi_3}^2}}$$
$$\times\left(1+L\phi_4^{\alpha}(d_1^2+\phi_4^2+2d_1\phi_4\phi_3)^{\frac{\alpha}{2}}\left(\ln\left(L\phi_4^{\alpha}(d_1^2+\phi_4^2+2d_1\phi_4\phi_3)^{\frac{\alpha}{2}}\right)+2c_0\right)\right) \tag{13}$$

$$\varphi_3 \approx \frac{\pi^2}{2MN}\sum_{m=1}^{M}\sum_{n=1}^{N}\sin\left(\frac{2m-1}{2M}\pi\right)\sin\left(\frac{2n-1}{2N}\pi\right)\Xi_{2\to\mathrm{far}}^{\mathrm{HD-CUP,cov}}\lambda_u{\phi_4}^{-3} e^{-\pi\lambda_u{\phi_4}^{-2}}\frac{1}{\sqrt{1-{\phi_3}^2}}$$
$$\times\left(1+L{\phi_4}^{-\alpha}(d_1^2+{\phi_4}^{-2}+2d_1{\phi_4}^{-1}\phi_3)^{\frac{\alpha}{2}}\left(\ln\left(L{\phi_4}^{-\alpha}(d_1^2+{\phi_4}^{-2}+2d_1{\phi_4}^{-1}\phi_3)^{\frac{\alpha}{2}}\right)+2c_0\right)\right) \tag{14}$$

$\left.\frac{e^{-J-K{\phi_4}^{-\alpha}}}{1-\mathcal{P}_{1\to\mathrm{far}}^{\mathrm{CUP}}}\right\}$ for $\{\varphi_1,\varphi_2,\varphi_3\}$ respectively, $J = \frac{\sigma^2\tau_2 d_1^{\alpha}}{P_a(a_f-a_n\tau_2)}$, $K = \frac{\sigma^2(\tau_2 a_n - a_f)}{P_u a_n}$, $L = \frac{\sigma^4 a_f}{a_n^2 P_u P_a}$, $\omega_3 = \sqrt{2}d_1\left(\frac{\phi_4}{\phi_3}-\phi_3\phi_4+\phi_3\right)$, $\phi_4 = \frac{1+\cos\left(\frac{2n-1}{2N}\pi\right)}{2}$.

Proof: The proof of (10) can refer to theorem 1 and is omitted here. We divide the original integration of $\underline{\mathcal{P}}_{2\to\mathrm{far}}^{\mathrm{HD-CUP}}$ into three parts due to the complexity of integral domain. For the detail of the proof, please refer to Appendix C. ■

Remark 3: When $\mathcal{U}_2$ is the far user, a_f should be above $\frac{\tau_2}{1+\tau_2}$. Combining the discussion in **Remark 2**, the feasible region of a_f with CUP scheme is $a_f \in \left(\max\{\frac{\tau_1}{1+\tau_1},\frac{\tau_2}{1+\tau_2}\},1\right)$, which guarantees that both paired users have positive average data rate. The monotonicity of (10)(11) can be discussed referring to **Remark 2** and is omitted here.

2) FD NOMA

In this subsection, we characterize the coverage probability of the user pair in FD NOMA networks.

Theorem 3: With CUP-based FD NOMA, when $\mathcal{U}_1$ is the far user, the coverage probability of $\mathcal{U}_2$ is obtained by replacing $\Xi_{2\to\mathrm{near}}^{\mathrm{HD-CUP,covI}}$, $\Xi_{2\to\mathrm{near}}^{\mathrm{HD-CUP,covII}}$ with

$$\Xi_{2\to\mathrm{near}}^{\mathrm{FD-CUP,covI}} = \frac{\sigma^2 e^{-A\omega_1}}{\left(\sigma^2+\mu A\kappa P_u\omega_1\right)\mathcal{P}_{1\to\mathrm{far}}^{\mathrm{CUP}}},$$
$$\Xi_{2\to\mathrm{near}}^{\mathrm{FD-CUP,covII}} = \frac{\sigma^2 e^{-A\omega_2}}{\left(\sigma^2+\mu A\kappa P_u\omega_2\right)\mathcal{P}_{1\to\mathrm{far}}^{\mathrm{CUP}}}$$

in (8). The coverage probability of $\mathcal{U}_1$ is obtained by replacing $\Xi_{1\to\mathrm{far}}^{\mathrm{HD-CUP,covI}}$, $\Xi_{1\to\mathrm{far}}^{\mathrm{HD-CUP,covII}}$ with

$$\Xi_{1\to\mathrm{far}}^{\mathrm{FD-CUP,covI}} = \frac{\sigma^2\, e^{-C\omega_1-D\left(\frac{\phi_1\phi_3}{\sqrt{2}}\right)^{\alpha}}}{\left(\sigma^2+\kappa\mu P_u C\omega_1\right)\mathcal{P}_{1\to\mathrm{far}}^{\mathrm{CUP}}},$$
$$\Xi_{1\to\mathrm{far}}^{\mathrm{FD-CUP,covII}} = \frac{\sigma^2\, e^{-C\omega_2-D\left(\frac{2\phi_1}{\phi_2+2\sqrt{2}}\right)^{\alpha}}}{\left(\sigma^2+\kappa\mu P_u C\omega_2\right)\mathcal{P}_{1\to\mathrm{far}}^{\mathrm{CUP}}}$$

in (9).

Proof: The probability density function (PDF) of channel gain h_u is $f_{h_u}(h) = \frac{1}{\mu}e^{-\frac{h}{\mu}}$. When the near user $\mathcal{U}_2$ is in the FD NOMA mode, the coverage probability of $\mathcal{U}_2$ is equivalent to introducing $\frac{\sigma^2}{\sigma^2+\mu A\kappa P_u d_2^{\alpha}}$ in (8). ■

Remark 4: The self-interference reduces the coverage probability of the FD NOMA system. The monotonicity of the coverage probability with respect to a_f is consistent with **Remark 2**. Besides, the coverage probability of both paired users decreases with κ and P_u. The near user should transmit with low power to resist self-interference whereas this leads to the degradation of far user rate.

When $\mathcal{U}_1$ is the near user, the coverage probability of $\mathcal{U}_1$ is

$$\mathcal{P}_{1\to\mathrm{near}}^{\mathrm{FD-CUP}} = \mathbf{1}(a_f > \frac{\tau_2}{1+\tau_2})\frac{\sigma^2 e^{-F}}{\sigma^2+\mu F\kappa P_u}. \tag{15}$$

The lower bound on the coverage probability of $\mathcal{U}_2$ is

$$\underline{\mathcal{P}}_{2\to\mathrm{far}}^{\mathrm{FD-CUP}} \approx \mathbf{1}(a_f > \frac{\tau_2}{1+\tau_2})\frac{\varphi_1+\varphi_2+\varphi_3}{1+\frac{\kappa\mu P_u\tau_2 d_1^{\alpha}}{P_a(a_f-a_n\tau_2)}}. \tag{16}$$

B. CSP SCHEME

With CSP scheme, we use the same polar coordinate as in Fig. 1. $\mathcal{U}_2$ is located at (r,θ), where $r = d_2, \theta = \angle\mathcal{U}_2\mathcal{S}\mathcal{U}_1 \in [-\frac{\pi}{2},\frac{\pi}{2}]$. Before evaluating coverage performance, we firstly give out the probability of $d_1 > d_2$.

Lemma 2: With CSP scheme, the probability that $\mathcal{U}_1$ serves as far user is

$$\mathcal{P}_{1\to\mathrm{far}}^{\mathrm{CSP}} = 1-e^{-\frac{\pi\lambda_u d_1^2}{2}}. \tag{17}$$

Proof: Since we have $-\frac{\pi}{2} \le \theta \le \frac{\pi}{2}$, the PDF of r is $f(r) = \lambda_u\pi r e^{-\frac{\lambda_u\pi r^2}{2}}$. Then (17) can be derived as in lemma 1. ■

Remark 5: When the density of user is large enough, $\mathcal{P}_{1\to\mathrm{far}}^{\mathrm{CSP}} \approx 1$.

1) HD NOMA

In this subsection, we characterize the coverage probability of the user pair in HD NOMA networks.

With CSP-based HD NOMA, when $\mathcal{U}_1$ is the far user, the coverage probability of $\mathcal{U}_2$ is approximated as

$$\mathcal{P}_{2\to\mathrm{near}}^{\mathrm{HD-CSP}} \approx \mathbf{1}(a_f > \frac{\tau_1}{1+\tau_1})\frac{\pi^2}{N}\sum_{n=1}^{N}\sin\left(\frac{2n-1}{2N}\pi\right) \times \Xi_{2\to\mathrm{near}}^{\mathrm{HD-CSP,cov}}\frac{\lambda_u\phi_1 d_1}{4}e^{-\frac{\pi\lambda_u\phi_1^2}{8}}, \quad (18)$$

where $\Xi_{2\to\mathrm{near}}^{\mathrm{HD-CSP,cov}} = \frac{e^{-A\left(\frac{\phi_1}{2}\right)^{\alpha}}}{\mathcal{P}_{1\to\mathrm{far}}^{\mathrm{CSP}}}$.

The lower bound on the coverage probability of $\mathcal{U}_1$ is

$$\underline{\mathcal{P}}_{1\to\mathrm{far}}^{\mathrm{HD-CSP}} \approx \mathbf{1}(a_f > \frac{\tau_1}{1+\tau_1})\frac{\pi^2}{MN}\sum_{m=1}^{M}\sum_{n=1}^{N}\sin\left(\frac{2n-1}{2N}\pi\right) \times \sin\left(\frac{2m-1}{2M}\pi\right)\Xi_{1\to\mathrm{far}}^{\mathrm{HD-CSP,cov}} \times \left(1+E\omega_4\left(\ln\left(E\omega_4\right)+2c_0\right)\right) \times \frac{\lambda_u d_1\phi_1}{4}e^{-\frac{\pi\lambda_u\phi_1^2}{8}}\frac{1}{\sqrt{1-\phi_3^2}}, \quad (19)$$

where

$$\Xi_{1\to\mathrm{far}}^{\mathrm{HD-CSP,cov}} = \frac{e^{-C\left(\frac{\phi_1}{2}\right)^{\alpha}-D\omega_4}}{\mathcal{P}_{1\to\mathrm{far}}^{\mathrm{CSP}}},$$

$$\omega_4 = \left(\frac{\phi_1^2}{4}+d_1^2-d_1\phi_1\phi_3\right)^{\frac{\alpha}{2}}.$$

When $\mathcal{U}_1$ is the near user, the coverage probability $\mathcal{P}_{1\to\mathrm{near}}^{\mathrm{HD-CSP}}$ is the same as $\mathcal{P}_{1\to\mathrm{near}}^{\mathrm{HD-CUP}}$. The lower bound on the coverage probability of $\mathcal{U}_2$ is

$$\underline{\mathcal{P}}_{2\to\mathrm{far}}^{\mathrm{HD-CSP}} \approx \mathbf{1}(a_f > \frac{\tau_2}{1+\tau_2})\frac{\pi^2}{MN}\sum_{m=1}^{M}\sum_{n=1}^{N}\sin\left(\frac{2n-1}{2N}\pi\right) \times \sin\left(\frac{2m-1}{2M}\pi\right)\Xi_{2\to\mathrm{far}}^{\mathrm{HD-CSP,cov}}\frac{\lambda_u\phi_5^3}{16d_1}e^{-\frac{\pi\lambda_u\phi_5^2}{8}}\frac{-1}{\sqrt{1-\phi_3^2}} \times \left(1+L\left(-\frac{\phi_5}{2}\right)^{\alpha}\omega_5\left(\ln\left(L\left(-\frac{\phi_5}{2}\right)^{\alpha}\omega_5\right)+2c_0\right)\right), \quad (20)$$

where

$$\Xi_{2\to\mathrm{far}}^{\mathrm{HD-CSP,cov}} = \frac{e^{-J-K\omega_5}}{1-\mathcal{P}_{1\to\mathrm{far}}^{\mathrm{CSP}}},$$

$$\omega_5 = \left(\frac{\phi_5^2}{4}+d_1^2+d_1\phi_3\phi_5\right)^{\frac{\alpha}{2}},$$

$$\phi_5 = \frac{4d_1}{\cos\left(\frac{2n-1}{2N}\pi\right)-1}.$$

2) FD NOMA

In this subsection, we characterize the coverage probability of the user pair in FD NOMA networks.

With CSP-based FD NOMA, when $\mathcal{U}_1$ is the far user, the coverage probability of $\mathcal{U}_2$ is obtained by replacing $\Xi_{2\to\mathrm{near}}^{\mathrm{HD-CSP,cov}}$ with

$$\Xi_{2\to\mathrm{near}}^{\mathrm{FD-CSP,cov}} = \frac{\sigma^2 e^{-A\left(\frac{\phi_1}{2}\right)^{\alpha}}}{\left(\sigma^2+\mu A\kappa P_u\left(\frac{\phi_1}{2}\right)^{\alpha}\right)\mathcal{P}_{1\to\mathrm{far}}^{\mathrm{CSP}}}$$

in (18). The coverage probability of $\mathcal{U}_1$ is obtained by replacing $\Xi_{1\to\mathrm{far}}^{\mathrm{HD-CSP,cov}}$ with

$$\Xi_{1\to\mathrm{far}}^{\mathrm{FD-CSP,cov}} = \frac{e^{-C\left(\frac{\phi_1}{2}\right)^{\alpha}-D\omega_4}}{\left(1+\frac{\kappa\mu P_u\tau_1\left(\frac{\phi_1}{2}\right)^{\alpha}}{P_a(a_f-a_n\tau_1)}\right)\mathcal{P}_{1\to\mathrm{far}}^{\mathrm{CSP}}}$$

in (19).

When $\mathcal{U}_1$ is the near user, the coverage probability of $\mathcal{U}_1$ is the same as $\mathcal{P}_{1\to\mathrm{near}}^{\mathrm{FD-CUP}}$. The lower bound on the coverage probability of $\mathcal{U}_2$ is obtained by replacing $\Xi_{2\to\mathrm{far}}^{\mathrm{HD-CSP,cov}}$ with

$$\Xi_{2\to\mathrm{far}}^{\mathrm{FD-CSP,cov}} = \frac{e^{-J-K\omega_5}}{\left(1+\frac{\kappa\mu P_u\tau_2 d_1^{\alpha}}{P_a(a_f-a_n\tau_2)}\right)\mathcal{P}_{1\to\mathrm{far}}^{\mathrm{CSP}}}$$

in (20).

The monotonicity of the coverage probability with CSP scheme is consistent with that with CUP scheme.

IV. AVERAGE DATA RATE

In this section, the average data rate of the cooperative NOMA system is analyzed with stochastic geometry and Gaussian-Chebyshev quadrature.

A. CUP SCHEME

The data rate at $\mathcal{U}_n, \mathcal{U}_f$ can be expressed as $\frac{1}{2}\log_2(1+\gamma_{n,n}^{\mathrm{H}})$ and $\frac{1}{2}\log_2(1+\gamma_{f,f}^{\mathrm{H}})$ with HD NOMA, and $\log_2(1+\gamma_{n,n}^{\mathrm{F}})$ and $\log_2(1+\gamma_{f,f}^{\mathrm{F}})$ with FD NOMA. In the following, we derive the average data rate of the user pair with CUP scheme in HD and FD NOMA networks respectively.

1) HD NOMA

In this subsection, we characterize the average data rate of the user pair in HD NOMA networks.

Theorem 4: With CUP-based HD NOMA, when $\mathcal{U}_1$ is the far user, the near user rate $\mathcal{R}_{2\to\mathrm{near}}^{\mathrm{HD-CUP}}$ is obtained by replacing $\Xi_{2\to\mathrm{near}}^{\mathrm{HD-CUP,covI}}$, $\Xi_{2\to\mathrm{near}}^{\mathrm{HD-CUP,covII}}$ with $\Xi_{2\to\mathrm{near}}^{\mathrm{HD-CUP,RI}}$, $\Xi_{2\to\mathrm{near}}^{\mathrm{HD-CUP,RII}}$ in (8), where

$$\Xi_{2\to\mathrm{near}}^{\mathrm{HD-CUP,RI}} = \frac{1}{2\ln 2\mathcal{P}_{1\to\mathrm{far}}^{\mathrm{CUP}}}\left[\ln(1+B)\,e^{-\frac{\sigma^2\tau_1}{P_a(a_f-a_n\tau_1)}\omega_1} - e^{\frac{\sigma^2}{a_nP_a}\omega_1}E_i\left[-\frac{\sigma^2}{a_nP_a}\omega_1(1+B)\right]\right],$$

$\Xi_{2\to\mathrm{near}}^{\mathrm{HD-CUP,RII}}$ equals to replacing ω_1 with ω_2 in $\Xi_{2\to\mathrm{near}}^{\mathrm{HD-CUP,RI}}$.

$$\mathcal{R}_{1\to\mathrm{far}}^{\mathrm{HD-CUP,OMA}} = \frac{\pi^2}{MN\mathcal{P}_{1\to\mathrm{far}}^{\mathrm{CUP}}}\sum_{m=1}^{M}\sum_{n=1}^{N}\sin\left(\frac{2m-1}{2M}\pi\right)\sin\left(\frac{2n-1}{2N}\pi\right)$$
$$\times\left[\frac{-e^{\frac{\sigma^2}{P_a}\omega_6+\frac{\sigma^2\phi_1^\alpha\phi_3^\alpha}{2^\alpha P_a}}E_i\left(-\frac{\sigma^2}{P_a}\omega_6-\frac{\sigma^2\phi_1^\alpha\phi_3^\alpha}{2^\alpha P_a}\right)}{2\ln 2\left(1-\frac{\phi_1^\alpha\phi_3^\alpha}{2^\alpha d_1^\alpha}\right)}\frac{d_1\left(\frac{P_u}{P_a}\right)^{\frac{2}{\alpha}}\lambda_u\phi_1\phi_3^2 e^{-\frac{\pi\lambda_u\phi_1^2\phi_3^2}{4}\left(\frac{P_u}{P_a}\right)^{\frac{2}{\alpha}}}}{\sqrt{4-\phi_3^2\left(\frac{P_u}{P_a}\right)^{\frac{2}{\alpha}}}}\right.$$
$$\left.+\frac{-e^{\frac{\sigma^2}{P_a}\omega_7+\frac{\sigma^2\phi_1^\alpha}{2^\alpha P_a}}E_i\left(-\frac{\sigma^2}{P_a}\omega_7-\frac{\sigma^2\phi_1^\alpha}{2^\alpha P_a}\right)}{2\ln 2\left(1-\frac{\phi_1^\alpha}{2^\alpha d_1^\alpha}\right)}\frac{d_1\left(\frac{P_u}{P_a}\right)^{\frac{2}{\alpha}}\lambda_u\phi_1 e^{-\frac{\pi\lambda_u\phi_1^2}{4}\left(\frac{P_u}{P_a}\right)^{\frac{2}{\alpha}}}\left(1-\frac{1}{2}\left(\frac{P_u}{P_a}\right)^{\frac{1}{\alpha}}\right)}{4\sqrt{1-\left[\phi_3\left(1-\frac{1}{2}\left(\frac{P_u}{P_a}\right)^{\frac{1}{\alpha}}\right)+\frac{1}{2}\left(\frac{P_u}{P_a}\right)^{\frac{1}{\alpha}}\right]^2}}\right] \quad (22)$$

The lower bound on the far user rate $\mathcal{R}_{1\to\mathrm{far}}^{\mathrm{HD-CUP}}$ is obtained by replacing $\Xi_{1\to\mathrm{far}}^{\mathrm{HD-CUP,covI}}$, $\Xi_{1\to\mathrm{far}}^{\mathrm{HD-CUP,covII}}$ with $\Xi_{1\to\mathrm{far}}^{\mathrm{HD-CUP,RI}}$, $\Xi_{1\to\mathrm{far}}^{\mathrm{HD-CUP,RII}}$ in (9), where

$$Xi_{1\to\mathrm{far}}^{\mathrm{HD-CUP,RI}} = -\frac{e^{-C\omega_1+\frac{\sigma^2}{a_nP_u}\left(\frac{\phi_1\phi_3}{\sqrt{2}}\right)^\alpha}}{2\ln 2\mathcal{P}_{1\to\mathrm{far}}^{\mathrm{CUP}}}E_i\left[-\frac{\sigma^2}{P_u}\left(\frac{\phi_1\phi_3}{\sqrt{2}}\right)^\alpha\right],$$
$$\Xi_{1\to\mathrm{far}}^{\mathrm{HD-CUP,RII}} = -\frac{e^{-C\omega_2+\frac{\sigma^2}{a_nP_u}\left(\frac{2\phi_1}{\phi_2+2\sqrt{2}}\right)^\alpha}}{2\ln 2\mathcal{P}_{1\to\mathrm{far}}^{\mathrm{CUP}}}E_i\left[-\frac{\sigma^2}{P_u}\left(\frac{2\phi_1}{\phi_2+2\sqrt{2}}\right)^\alpha\right].$$

Proof: Please refer to Appendix D. ■

When $\mathcal{U}_1$ is the near user, the near user rate $\mathcal{R}_{1\to\mathrm{near}}^{\mathrm{HD-CUP}}$ is

$$\mathcal{R}_{1\to\mathrm{near}}^{\mathrm{HD-CUP}} = \frac{\mathbf{1}(a_f>\frac{\tau_2}{1+\tau_2})}{2\ln 2}\times\left[\ln(1+G)\,e^{-\frac{\sigma^2\tau_2}{P_a(a_f-a_n\tau_2)}d_1^\alpha} - e^{\frac{\sigma^2}{a_nP_a}d_1^\alpha}E_i\left[-\frac{\sigma^2 d_1^\alpha}{a_nP_a}(1+G)\right]\right]. \quad (21)$$

The far user rate $\mathcal{R}_{2\to\mathrm{far}}^{\mathrm{HD-CUP}}$ is obtained by replacing $\Xi_{2\to\mathrm{far}}^{\mathrm{HD-CUP,cov}}$ with $\Xi_{2\to\mathrm{far}}^{\mathrm{HD-CUP,R}}$ in (11), where

$$\Xi_{2\to\mathrm{far}}^{\mathrm{HD-CUP,R}} = \left\{-\frac{e^{-J+\frac{\sigma^2}{a_nP_u}\omega_3^\alpha}}{2\ln 2(1-\mathcal{P}_{1\to\mathrm{far}}^{\mathrm{CUP}})}E_i\left[-\frac{\sigma^2}{P_u}\omega_3^\alpha\right],\ -\frac{e^{-J+\frac{\sigma^2}{a_nP_u}\phi_4^\alpha}}{2\ln 2(1-\mathcal{P}_{1\to\mathrm{far}}^{\mathrm{CUP}})}E_i\left[-\frac{\sigma^2}{P_u}\phi_4^\alpha\right],\ -\frac{e^{-J+\frac{\sigma^2}{a_nP_u}\phi_4^{-\alpha}}}{2\ln 2(1-\mathcal{P}_{1\to\mathrm{far}}^{\mathrm{CUP}})}E_i\left[-\frac{\sigma^2}{P_u}\phi_4^{-\alpha}\right]\right\}$$

for $\{\varphi_1, \varphi_2, \varphi_3\}$ respectively.

Remark 6: The far user rate increases with growing a_f. With high SNR regime, i.e., $\frac{P_a}{\sigma^2}\to\infty$ and $\frac{P_a}{\sigma^2}=t\frac{P_u}{\sigma^2}$, the average data rate of CUP-based HD NOMA can be approximated as

$$\Xi_{2\to\mathrm{near}}^{\mathrm{HD-CUP},\infty} = \frac{\ln\left(1+\frac{a_n\tau_1}{1-a_n(1+\tau_1)}\right)-E_i[0]}{2\ln 2\mathcal{P}_{1\to\mathrm{far}}^{\mathrm{CUP}}},$$
$$\Xi_{1\to\mathrm{far}}^{\mathrm{HD-CUP},\infty} = -\frac{E_i[0]}{2\ln 2\mathcal{P}_{1\to\mathrm{far}}^{\mathrm{CUP}}}, E=0,$$
$$\mathcal{R}_{1\to\mathrm{near}}^{\mathrm{HD-CUP},\infty} = \frac{1}{2\ln 2}\left[\ln\left(1+\frac{a_n\tau_2}{1-a_n(1+\tau_2)}\right)-E_i[0]\right],$$
$$\Xi_{2\to\mathrm{far}}^{\mathrm{HD-CUP},\infty} = -\frac{E_i[0]}{2\ln 2(1-\mathcal{P}_{1\to\mathrm{far}}^{\mathrm{CUP}})}, L=0.$$

We observe that the near user rate decreases with a_f due to less remaining power for near user's own signal. The far user rate remains as a constant since it is dominated by the relaying link and is unrelated to a_f. Therefore, the sum rate decreases with a_f.

Remark 7: When $\tau_i \geq \tau_j$ ($\{i,j\}\in\{1,2\}, i\neq j$) and $a_f\to\max\{\frac{\tau_1}{1+\tau_1},\frac{\tau_2}{1+\tau_2}\}=\frac{\tau_i}{1+\tau_i}$, the average data rate is $\mathcal{R}_{i\to\mathrm{far}}^{\mathrm{HD-CUP}}=0$, $\mathcal{R}_{j\to\mathrm{near}}^{\mathrm{HD-CUP}}=0$. This is because, when $\mathcal{U}_i$ is the far user and $\mathcal{S}$ allocates minimum possible power to the far user, it is difficult to decode x_i at the near user.

When $a_f\to 1$, $\mathcal{S}$ allocates maximum power to the far user, the NOMA system transforms to an OMA system where $\mathcal{U}_n$ only serves as a helper of $\mathcal{U}_f$ and does not receive its own message. The far user rate holds as a constant. For example, when $\mathcal{U}_1$ is the far user, the far user rate is given by (22), as shown at the top of this page, where

$$\omega_6 = \left(\frac{\phi_1^2\phi_3^2}{4}\left(\frac{P_u}{P_a}\right)^{\frac{2}{\alpha}}+d_1^2-\frac{\phi_1\phi_3^2 d_1}{2}\left(\frac{P_u}{P_a}\right)^{\frac{2}{\alpha}}\right)^{\frac{\alpha}{2}},$$
$$\omega_7 = \left(\frac{\phi_1^2}{4}\left(\frac{P_u}{P_a}\right)^{\frac{2}{\alpha}}+d_1^2-\phi_1 d_1\left(\frac{P_u}{P_a}\right)^{\frac{1}{\alpha}}\times\left(\phi_3\left(1-\frac{1}{2}\left(\frac{P_u}{P_a}\right)^{\frac{1}{\alpha}}\right)+\frac{1}{2}\left(\frac{P_u}{P_a}\right)^{\frac{1}{\alpha}}\right)\right)^{\frac{\alpha}{2}}.$$

2) FD NOMA

In this subsection, we characterize the average data rate of the user pair in FD NOMA networks.

With CUP-based FD NOMA, when $\mathcal{U}_1$ is the far user, the near user rate $\mathcal{R}_{2\to near}^{FD-CUP}$ is obtained by replacing $\Xi_{2\to near}^{HD-CUP,covI}$, $\Xi_{2\to near}^{HD-CUP,covII}$ with $\Xi_{2\to near}^{FD-CUP,RI}$, $\Xi_{2\to near}^{FD-CUP,RII}$ in (8), where

$$\Xi_{2\to near}^{FD-CUP,RI} = \frac{1}{\ln 2\mathcal{P}_{1\to far}^{HD-CUP}}\left[\ln(1+B)\frac{e^{-\frac{\sigma^2\tau_1}{P_a(a_f-a_n\tau_1)}\omega_1}}{1+\frac{\mu\tau_1\kappa P_u\omega_1}{P_a(a_f-a_n\tau_1)}}\right.$$

$$\left.+\frac{\pi}{Q}\sum_{q=1}^{Q}\sin\left(\frac{2q-1}{2Q}\pi\right)\frac{B\phi_6^2 e^{-\frac{\sigma^2 B}{a_nP_a}\phi_6\omega_1}}{2(1+B\phi_6)\left(1+\frac{\mu B\phi_6\kappa P_u\omega_1}{a_nP_a}\right)}\right],$$

$\Xi_{2\to near}^{FD-CUP,RII}$ equals to replacing ω_1 with ω_2 in $\Xi_{2\to near}^{FD-CUP,RI}$, $\phi_6 = \frac{2}{1-\cos\left(\frac{2q-1}{2Q}\pi\right)}$.

The lower bound on the far user rate $\mathcal{R}_{1\to far}^{FD-CUP}$ is obtained by replacing $\Xi_{1\to far}^{HD-CUP,covI}$, $\Xi_{1\to far}^{HD-CUP,covII}$ with $\Xi_{1\to far}^{FD-CUP,RI}$, $\Xi_{1\to far}^{FD-CUP,RII}$ in (9), where

$$\Xi_{1\to far}^{FD-CUP,RI} = -\frac{\sigma^2 e^{-C\omega_1+\frac{\sigma^2}{a_nP_u}\left(\frac{\phi_1\phi_3}{\sqrt{2}}\right)^\alpha}}{\ln 2\mathcal{P}_{1\to far}^{CUP}(\sigma^2+\kappa\mu P_uC\omega_1)}E_i\left[-\frac{\sigma^2}{P_u}\left(\frac{\phi_1\phi_3}{\sqrt{2}}\right)^\alpha\right],$$

$$\Xi_{1\to far}^{FD-CUP,RII} = -\frac{\sigma^2 e^{-C\omega_2+\frac{\sigma^2}{a_nP_u}\left(\frac{2\phi_1}{\phi_2+2\sqrt{2}}\right)^\alpha}}{\ln 2\mathcal{P}_{1\to far}^{CUP}(\sigma^2+\kappa\mu P_uC\omega_2)}E_i\left[-\frac{\sigma^2}{P_u}\left(\frac{2\phi_1}{\phi_2+2\sqrt{2}}\right)^\alpha\right].$$

When $\mathcal{U}_1$ is the near user, the near user rate is

$$\mathcal{R}_{1\to near}^{FD-CUP} = \frac{\mathbf{1}(a_f>\frac{\tau_2}{1+\tau_2})}{\ln 2}\left[\ln(1+G)\frac{e^{-\frac{\sigma^2\tau_2}{P_a(a_f-a_n\tau_2)}d_1^\alpha}}{1+\frac{\kappa\mu P_u\tau_2 d_1^\alpha}{P_a(a_f-a_n\tau_2)}}\right.$$

$$\left.+\frac{\pi}{Q}\sum_{n=1}^{Q}\sin\left(\frac{2n-1}{2Q}\pi\right)\frac{G\phi_6^2 e^{-\frac{\sigma^2 G}{a_nP_a}\phi_6 d_1^\alpha}}{2(1+G\phi_6)\left(1+\frac{\mu G\phi_6\kappa P_u d_1^\alpha}{a_nP_a}\right)}\right]. \quad (23)$$

The far user rate $\mathcal{R}_{2\to far}^{FD-CUP}$ is obtained by replacing $\Xi_{2\to far}^{HD-CUP,cov}$ with $\Xi_{2\to far}^{FD-CUP,R}$ in (11), where

$$\Xi_{2\to far}^{FD-CUP,R} = \left\{-\frac{e^{-J+\frac{\sigma^2}{a_nP_u}\omega_3^\alpha}E_i\left[-\frac{\sigma^2}{P_u}\omega_3^\alpha\right]}{\ln 2\left(1-\mathcal{P}_{1\to far}^{CUP}\right)\left(1+\frac{\kappa\mu P_u\tau_2 d_1^\alpha}{P_a(a_f-a_n\tau_2)}\right)},\right.$$

$$-\frac{e^{-J+\frac{\sigma^2}{a_nP_u}\phi_4^\alpha}E_i\left[-\frac{\sigma^2}{P_u}\phi_4^\alpha\right]}{\ln 2\left(1-\mathcal{P}_{1\to far}^{CUP}\right)\left(1+\frac{\kappa\mu P_u\tau_2 d_1^\alpha}{P_a(a_f-a_n\tau_2)}\right)},$$

$$\left.-\frac{e^{-J+\frac{\sigma^2}{a_nP_u}\phi_4^{-\alpha}}E_i\left[-\frac{\sigma^2}{P_u}\phi_4^{-\alpha}\right]}{\ln 2\left(1-\mathcal{P}_{1\to far}^{CUP}\right)\left(1+\frac{\kappa\mu P_u\tau_2 d_1^\alpha}{P_a(a_f-a_n\tau_2)}\right)}\right\}$$

for $\{\varphi_1, \varphi_2, \varphi_3\}$ respectively.

Remark 8: With CUP-based FD NOMA, the far user rate increases with a_f and decreases with κ and P_u. The monotonicity of the near user rate with respect to a_f is not clear. We evaluate the effect of a_f on the near user rate via numerical simulation.

B. CSP SCHEME

1) HD NOMA

In this subsection, we characterize the average data rate of the user pair in HD NOMA networks.

When $\mathcal{U}_1$ is the far user, the near user rate $\mathcal{R}_{2\to near}^{HD-CSP}$ is obtained by replacing $\Xi_{2\to near}^{HD-CSP,cov}$ with $\Xi_{2\to near}^{HD-CSP,R}$ in (18), where

$$\Xi_{2\to near}^{HD-CSP,R} = \frac{1}{2\ln 2\mathcal{P}_{1\to far}^{CSP}}\left[\ln(1+B)\,e^{-\frac{\sigma^2\tau_1}{P_a(a_f-a_n\tau_1)}\left(\frac{\phi_1}{2}\right)^\alpha}\right.$$

$$\left.-e^{\frac{\sigma^2}{a_nP_a}\left(\frac{\phi_1}{2}\right)^\alpha}E_i\left[-\frac{\sigma^2}{a_nP_a}\left(\frac{\phi_1}{2}\right)^\alpha(1+B)\right]\right].$$

The far user rate $\mathcal{R}_{1\to far}^{HD-CSP}$ is obtained by replacing $\Xi_{1\to far}^{HD-CSP,cov}$ with $\Xi_{1\to far}^{HD-CSP,R}$ in (19), where

$$\Xi_{1\to far}^{HD-CSP,R} = -\frac{e^{-C\left(\frac{\phi_1}{2}\right)^\alpha}e^{\frac{\sigma^2}{a_nP_u}\omega_4}E_i\left[-\frac{\sigma^2}{P_u}\omega_4\right]}{2\ln 2\mathcal{P}_{1\to far}^{CSP}}.$$

When $\mathcal{U}_1$ is the near user, the near user rate $\mathcal{R}_{1\to near}^{HD-CSP}$ is the same as $\mathcal{R}_{1\to near}^{HD-CUP}$. The far user rate $\mathcal{R}_{2\to far}^{HD-CSP}$ is obtained by replacing $\Xi_{2\to far}^{HD-CSP,cov}$ with $\Xi_{2\to far}^{HD-CSP,R}$ in (20), where

$$\Xi_{2\to far}^{HD-CSP,R} = -\frac{e^{-J+\frac{\sigma^2}{a_nP_u}\omega_5}}{2\ln 2\left(1-\mathcal{P}_{1\to far}^{CSP}\right)}E_i\left[-\frac{\sigma^2}{P_u}\omega_5\right].$$

Remark 9: With CSP-based HD NOMA, the high SNR approximations of the data rate can be obtained as in **Remark 6** and the monotonicity of the high SNR approximations is consistent with that in **Remark 6**.

2) FD NOMA

In this subsection, we characterize the average data rate of the user pair in FD NOMA networks.

When $\mathcal{U}_1$ is the far user, the near user rate $\mathcal{R}_{2\to\text{near}}^{\text{FD}-\text{CSP}}$ is obtained by replacing $\Xi_{2\to\text{near}}^{\text{HD}-\text{CSP},\text{cov}}$ with $\Xi_{2\to\text{near}}^{\text{FD}-\text{CSP},\text{R}}$ in (18), where

$$\begin{aligned}
&\Xi_{2\to\text{near}}^{\text{FD}-\text{CSP},\text{R}} \\
&= \frac{1}{\ln 2\mathcal{P}_{1\to\text{far}}^{\text{CSP}}} \\
&\quad\times\Bigg[\ln(1+B)\, e^{-\frac{\sigma^2\tau_1}{P_a(a_f-a_n\tau_1)}\left(\frac{\phi_1}{2}\right)^{\alpha}} \frac{1}{1+\frac{\mu\tau_1\kappa P_u}{P_a(a_f-a_n\tau_1)}\left(\frac{\phi_1}{2}\right)^{\alpha}} \\
&\quad + \frac{\pi}{Q}\sum_{q=1}^{Q}\sin\left(\frac{2q-1}{2Q}\pi\right)\frac{B\phi_6^2 e^{-\frac{\sigma^2 B}{a_n P_a}\phi_6\left(\frac{\phi_1}{2}\right)^{\alpha}}}{2\left(1+B\phi_6\right)\left(1+\frac{\mu B\phi_6\kappa P_u}{a_n P_a}\left(\frac{\phi_1}{2}\right)^{\alpha}\right)}\Bigg].
\end{aligned}$$

The far user rate $\underline{\mathcal{R}}_{1\to\text{far}}^{\text{FD}-\text{CSP}}$ is obtained by replacing $\Xi_{1\to\text{far}}^{\text{HD}-\text{CSP},\text{cov}}$ with $\Xi_{1\to\text{far}}^{\text{FD}-\text{CSP},\text{R}}$ in (19), where

$$\Xi_{1\to\text{far}}^{\text{FD}-\text{CSP},\text{R}} = -\frac{e^{-C\left(\frac{\phi_1}{2}\right)^{\alpha}+\frac{\sigma^2}{a_n P_u}\omega_4} E_i\left[-\frac{\sigma^2}{P_u}\omega_4\right]}{\ln 2\mathcal{P}_{1\to\text{far}}^{\text{CSP}}\left(1+\frac{\kappa\mu P_u\tau_1\left(\frac{\phi_1}{2}\right)^{\alpha}}{P_a(a_f-a_n\tau_1)}\right)}.$$

When $\mathcal{U}_1$ is the near user, the near user rate $\mathcal{R}_{1\to\text{near}}^{\text{FD}-\text{CSP}}$ is the same as $\mathcal{R}_{1\to\text{near}}^{\text{FD}-\text{CUP}}$. The far user rate $\underline{\mathcal{R}}_{2\to\text{far}}^{\text{FD}-\text{CSP}}$ is obtained by replacing $\Xi_{2\to\text{far}}^{\text{HD}-\text{CSP},\text{cov}}$ with $\Xi_{2\to\text{far}}^{\text{FD}-\text{CSP},\text{R}}$ in (20), where

$$\Xi_{2\to\text{far}}^{\text{FD}-\text{CSP},\text{R}} = -\frac{e^{-J+\frac{\sigma^2}{a_n P_u}\omega_5} E_i\left[-\frac{\sigma^2}{P_u}\omega_5\right]}{\ln 2\left(1-\mathcal{P}_{1\to\text{far}}^{\text{CSP}}\right)\left(1+\frac{\kappa\mu P_u\tau_2 d_1^{\alpha}}{P_a(a_f-a_n\tau_2)}\right)}.$$

Therefore, the lower bound on the sum rate of Y (Y ∈ {HD, FD}) NOMA system with Z (Z ∈ {CUP, CSP}) scheme is

$$\begin{aligned}
\underline{\mathcal{R}}_{\text{sum}}^{\text{Y}-\text{Z}} \approx\ & \mathcal{P}_{1\to\text{far}}^{\text{Z}}\left(\mathcal{R}_{2\to\text{near}}^{\text{Y}-\text{Z}}+\underline{\mathcal{R}}_{1\to\text{far}}^{\text{Y}-\text{Z}}\right) \\
&+\left(1-\mathcal{P}_{1\to\text{far}}^{\text{Z}}\right)\left(\underline{\mathcal{R}}_{2\to\text{far}}^{\text{Y}-\text{Z}}+\mathcal{R}_{1\to\text{near}}^{\text{Y}-\text{Z}}\right).
\end{aligned} \quad (24)$$

V. NUMERICAL RESULTS

In this section, we numerically evaluate the validity of the analytical results and investigate the impact of user pairing, transmission mode and power allocation on the system performance. We provide the performance of non-cooperative NOMA and OMA systems for comparison. Based on the conclusion in [16], only CSP scheme is considered in the non-cooperative NOMA system. For the OMA system, as in [8], $\mathcal{S}$ serves paired users in the TDMA mode. The transmission duration is divided into two phases with equal length. In the first phase, $\mathcal{S}$ transmits x_n to $\mathcal{U}_n$. In the second phase, $\mathcal{S}$ transmits x_f to $\mathcal{U}_f$ and $\mathcal{U}_n$ acts as an FD DF relay for the transmission. The performance analysis for the OMA system is equivalent to let $a_n = 1$ in the first phase and let $a_f = 1$ in the second phase in the FD NOMA system, which can be performed referring to **Remark 7**.

For each transmission scheme, the optimal power allocation (i.e., the optimal a_f and P_u) that maximizes the data rate performance is obtained via exhaustive search. It is difficult to derive the closed form solution of the optimal power allocation due to the linear combinations of exponential functions. With the optimal power allocation, the best transmission scheme is obtained by comparing the maximum data rate of each transmission scheme.

A. SYSTEM PARAMETERS AND SIMULATION SETUP

The following system parameters are considered unless specified. $\mathcal{U}_1$ is located at the distance $d_1 = 30$ meters (m) of $\mathcal{S}$. The density of candidate users is $\lambda_u = 4000/\text{km}^2$. The maximum transmit power of $\mathcal{S}$ and user is 33dBm and 23dBm, respectively [32], [33]. The channel fading gain h_u follows exponential distribution with average power $\mu = 0.1$ [6] and the path loss exponent α is 4. We set the noise average power, inter-user interference, self-interference cancelation factor to be $\sigma_0^2 = -104$dBm, $I_{\text{inter}} = -90$dBm [26], $\kappa = 10^{-6}$ respectively. The target data rate of x_1 and x_2 is 1bps/Hz. Correspondingly, the target SINR thresholds are $\tau_1 = \tau_2 = 1$ for FD NOMA and non-cooperative NOMA systems, and $\tau_1 = \tau_2 = 3$ for HD NOMA and OMA systems. The linear combination constants N, M, Q are 30 to obtain relatively accurate results with moderate computational complexity. Monte Carlo simulations with 10^6 independent experiments are conducted.

B. EFFECT OF TRANSMIT POWER AND POWER ALLOCATION COEFFICIENT

1) COVERAGE PROBABILITY

Fig. 5 shows the coverage probability of different transmission schemes against P_a. The analytical results are consistent with the simulations. The coverage probability of CSP scheme outperforms that of CUP scheme in both HD NOMA and FD NOMA systems due to that the received signals at $\mathcal{U}_n$

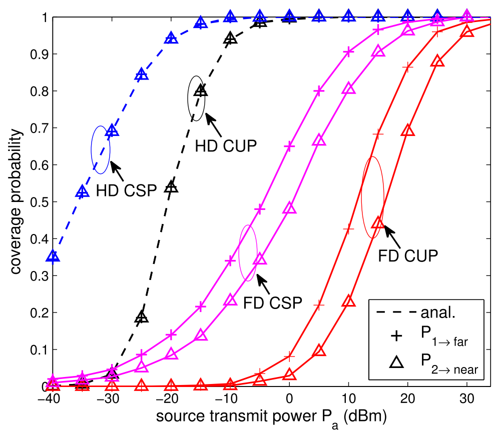

FIGURE 5. Comparison of the coverage probability with different transmission schemes versus P_a, where $a_f = 0.8$, $P_u = 23$ dBm.

experience less path loss with CSP scheme. HD NOMA outperforms FD NOMA in terms of coverage probability. This is because the self-interference introduced by FD NOMA is large compared with the power of desired signals, resulting in the degradation of SINR at $\mathcal{U}_n$. When P_a is large enough, both near user and far user are with high coverage probability in the cooperative NOMA system.

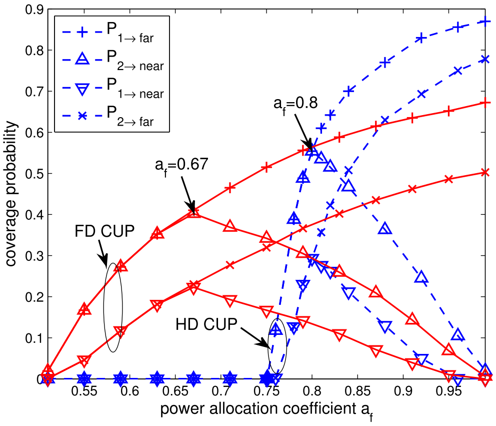

FIGURE 6. Comparison of the coverage probability with different transmission schemes versus a_f, where $P_a = -20$ dBm, $P_u = -10$ dBm.

Fig. 6 shows the coverage probability of CUP-based cooperative NOMA against a_f with low transmit SNR. As the analysis in **Remark 3**, $a_f > \max\{\frac{\tau_1}{1+\tau_1}, \frac{\tau_2}{1+\tau_2}\}$ (i.e., $a_f > 0.75$ for HD NOMA, $a_f > 0.5$ for FD NOMA) ensures positive coverage probability at paired users. With CUP-based HD NOMA (FD NOMA), the coverage probability of the near user increases with growing a_f when $a_f \in (0.75, 0.8]$ ($a_f \in (0.5, 0.67]$), and decreases with growing a_f when $a_f \in (0.8, 1)$ ($a_f \in (0.67, 1)$). The coverage probability of the far user always increases with growing a_f. These observations are identical with the discussion in **Remark 2**.

2) AVERAGE DATA RATE

Fig. 7 describes the sum data rate of different transmission schemes against P_u. There exists an extreme point of the sum data rate for CUP-based FD NOMA. When P_u is small, the decrease of P_u reduces far user rate dramatically and the sum data rate becomes lower. When P_u is relatively large, the increase of P_u improves far user rate but produces severer self-interference. The improvement of far user rate cannot compensate the loss of near user rate, further resulting in the decrease of the sum data rate. In the HD NOMA system, the sum data rate increases with growing P_u because the increase of P_u improves far user rate.

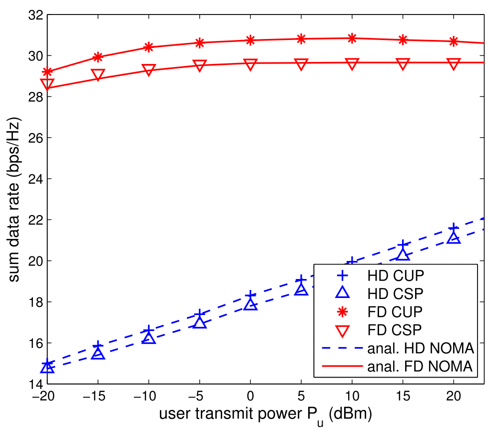

FIGURE 7. Comparison of the sum data rate with different transmission schemes versus P_u, where $a_f = 0.8$, $P_a = 33$ dBm.

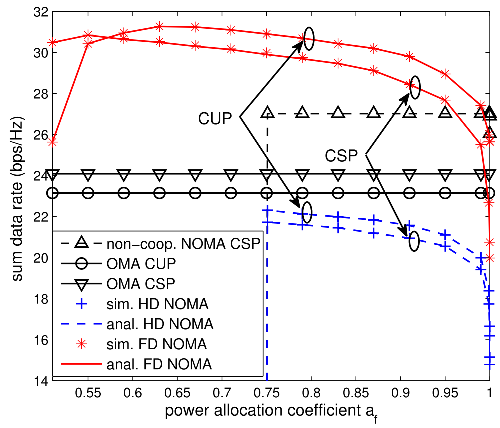

FIGURE 8. Comparison of the sum data rate with different transmission schemes versus a_f, where $P_a = 33$ dBm, $P_u = 23$ dBm.

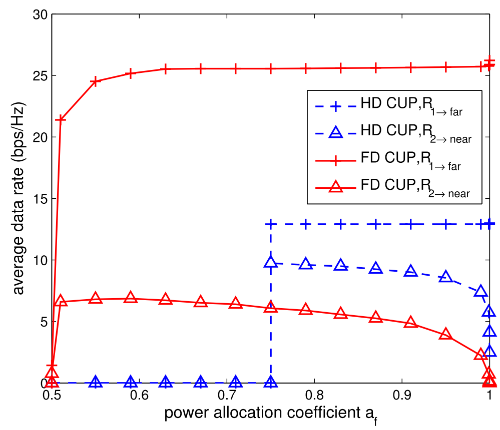

FIGURE 9. Comparison of the average data rate with different transmission schemes versus a_f, where $P_a = 33$ dBm, $P_u = 23$ dBm.

Fig. 8 and Fig. 9 demonstrate the sum data rate and average data rate of different transmission schemes versus a_f. When a_f is relatively large, the sum data rate of both HD NOMA and FD NOMA systems decreases with a_f. This is due to that with growing a_f, less remaining power for x_n reduces near user rate, and the far user rate determined by the relaying link almost remains as a constant. This observation verifies the conclusion in **Remark 6**. The sum data rate of CUP-based FD NOMA outperforms that of other transmission schemes. For CUP-based FD NOMA, the slight path loss of $\mathcal{U}_n$-$\mathcal{U}_f$ link enlarges far user rate significantly, besides, the extended transmission duration of FD NOMA benefits the improvement of the sum data rate. With CUP-based cooperative NOMA, the minimum user rate is determined by the near user rate. When $a_f \to \max\{\frac{\tau_1}{1+\tau_1}, \frac{\tau_2}{1+\tau_2}\}$, the average data rate of paired users is zero. When $a_f \to 1$, the near user rate is zero and the far user rate holds as a constant, which is consistent with the conclusion in **Remark 7**.

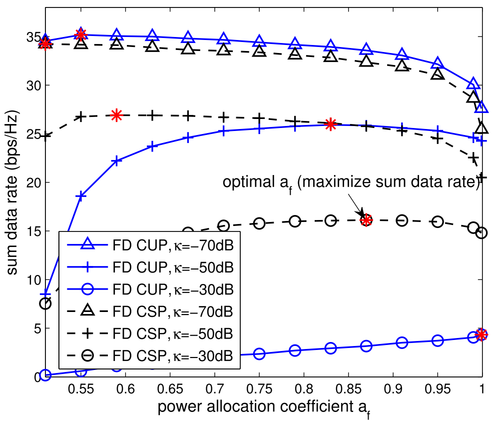

FIGURE 10. Comparison of the sum data rate with CUP-based and CSP-based FD NOMA versus a_f, where $P_a = 33$ dBm, $P_u = 23$ dBm.

Fig. 10 shows the sum data rate of CUP-based and CSP-based FD NOMA versus a_f. With the increase of κ, the sum data rate of the user pair reduces due to severer self-interference. When $\kappa = -70$dB (i.e., with strong self-interference cancelation capability), CUP-based FD NOMA outperforms CSP-based FD NOMA in terms of the sum data rate. As κ grows, the conclusion reverses since severe self-interference jointly with large path loss of $\mathcal{S}$-$\mathcal{U}_n$ link makes it difficult to decode x_f at the near user in the CUP-based FD NOMA system. Moreover, there exists an extreme point of the sum data rate for each transmission scheme. The optimal a_f that maximizes the sum data rate increases with growing κ. When κ increases, aiming to maximize the sum data rate, the decoding of x_f at the near user should be guaranteed, thus more power is allocated to x_f to resist the increasing self-interference.

C. EFFECT OF USER LOCATION AND USER DENSITY

Fig. 11 and Fig. 12 show maximum minimum user rate and maximum sum data rate of different transmission schemes against λ_u. The maximum minimum user rate of CUP-based FD NOMA (i.e., maximum near user rate) increases with λ_u. With growing λ_u, the increasing path loss of $\mathcal{S}$-$\mathcal{U}_n$ link results in the loss of near user rate, but the decrease of P_u can reduce self-interference and compensate the loss of near user rate, meanwhile sacrificing only a small degree of far user rate. Differently, the maximum minimum user rate of CSP-based FD NOMA (i.e., maximum far user rate) increases with λ_u due to the increase of a_f and P_u. When P_u reaches maximum value (i.e., λ_u is larger than approximate 28000/km^2), the maximum minimum user rate begins to decrease with λ_u.

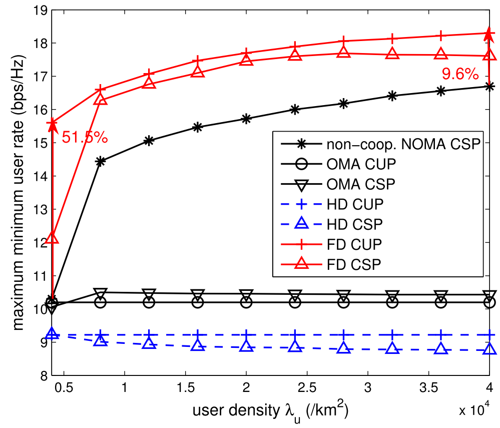

FIGURE 11. Comparison of the maximum minimum user rate with different transmission schemes versus λ_u, where $P_a = 33$ dBm.

With CSP-based HD NOMA, the near user transmits at maximum power and the maximum minimum user rate (i.e., maximum far user rate) decreases with λ_u since higher a_f cannot compensate the loss of far user rate caused by the increasing path loss of the relaying link.

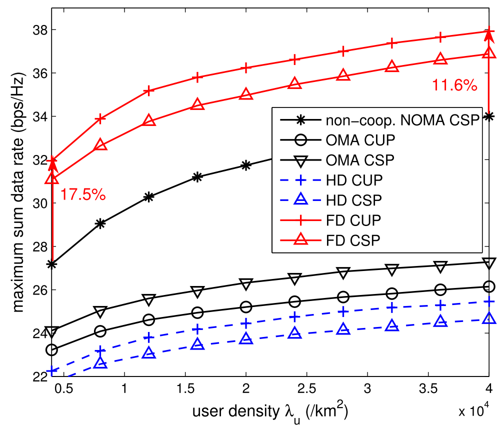

FIGURE 12. Comparison of the maximum sum data rate with different transmission schemes versus λ_u, where $P_a = 33$ dBm.

Combining the results in Fig. 11 and Fig. 12, we conclude that CUP-based cooperative NOMA achieves higher sum data rate and minimum user rate than CSP-based cooperative NOMA, which is distinct from the conclusion in the non-cooperative NOMA system [16]. When $d_1 = 30$m, CUP-based FD NOMA is the best transmission scheme that maximizes the minimum user rate as well as sum data rate. CUP-based FD NOMA outperforms CSP-based non-cooperative NOMA with approximate 51.5% and 9.6% gain on maximum minimum user rate in less dense scenario and dense scenario respectively, and with 17.5% and 11.6% gain on maximum sum data rate in these two scenarios. The OMA system performs worse than FD NOMA and non-cooperative NOMA systems in terms of the data rate performance.

Fig. 13 describes the best transmission scheme that maximizes the minimum user rate with varying d_1 and λ_u.

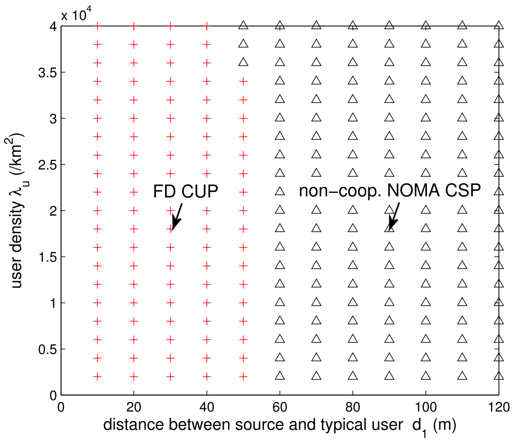

FIGURE 13. The best transmission scheme that maximizes the minimum user rate with different d_1 and λ_u, where $P_a = 33$ dBm.

CUP-based FD NOMA is the best transmission scheme with $\mathcal{U}_1$ close to $\mathcal{S}$. When $d_1 < 50$m, with CUP-based FD NOMA, the existence of the relaying link improves far user rate significantly and comparatively large near user rate can be achieved via reducing P_u. Besides, the extended transmission duration of FD NOMA improves the data rate compared with HD NOMA and OMA systems. CSP-based non-cooperative NOMA is the best transmission scheme with $\mathcal{U}_1$ far from $\mathcal{S}$. When $d_1 > 50$m, the near user rate decreases rapidly with the increase of d_1 in the CUP-based FD NOMA system. For CSP-based non-cooperative NOMA, the increase of a_f contributes to the performance gain on far user rate and the short distance of $\mathcal{S}$-$\mathcal{U}_n$ link ensures comparatively large near user rate, thus higher minimum user rate is achieved.

VI. CONCLUSION

In this paper, we have investigated the coverage and data rate performance of CUP and CSP schemes in HD NOMA and FD NOMA networks, and explored the impact of user pairing, transmission mode and power allocation on the system performance. Lower bounds on the coverage probability and average data rate are derived using stochastic geometry and Gaussian-Chebyshev quadrature. Numerical results indicate that CUP-based cooperative NOMA outperforms CSP-based cooperative NOMA in terms of the sum data rate as well as the minimum user rate, which reveals a new direction in the design of cooperative NOMA systems. CUP-based FD NOMA and CSP-based non-cooperative NOMA are the best transmission schemes with typical user close to and far from the source, respectively.

The conclusions obtained in this paper rely on the assumption of single antenna. A promising future direction is to consider user pairing in multi-antenna scenarios. Since the channel gains are vectors, it is challenging to perform antenna selection and decide the decoding order of SIC. The joint design of antenna selection, user pairing and power allocation will be studied to further improve the performance of the NOMA users.

APPENDIX A
PROOF OF LEMMA 1

The PDF of r is $f(r) = 2\pi\lambda_u r e^{-\pi\lambda_u r^2}$ [34]. Based on the cosine theorem, d_2 can be represented as $d_2 = \left(r^2+d_1^2+2rd_1\cos\theta\right)^{\frac{1}{2}}$. The probability that $\mathcal{U}_1$ serves as far user is

$$
\begin{aligned}
\mathcal{P}_{1\to\text{far}}^{\text{CUP}} &= \Pr\left(d_2 < d_1\right) \\
&= \frac{1}{2\pi}\int_{\frac{\pi}{2}}^{\frac{3\pi}{2}}\int_0^{\min\left\{-2d_1\cos\theta,-\frac{d_1}{\cos\theta}\right\}} f(r)drd\theta \\
&= \int_{\frac{\pi}{2}}^{\frac{3\pi}{4}}\int_0^{-2d_1\cos\theta}\frac{f(r)}{\pi}drd\theta \\
&\quad + \int_{\frac{3\pi}{4}}^{\pi}\int_0^{-\frac{d_1}{\cos\theta}}\frac{f(r)}{\pi}drd\theta. \qquad (25)
\end{aligned}
$$

Then, (7) is obtained by employing $u = \pi - \theta$, $v = 2\sqrt{2}\cos u - 1$, $v = \frac{4\cos u - 2\sqrt{2}}{2-\sqrt{2}} - 1$ and Gaussian-Chebyshev quadrature.

APPENDIX B
PROOF OF THEOREM 1

When $\mathcal{U}_1$ is the far user, $\mathcal{U}_2$ is in coverage when $\mathcal{U}_2$ can successfully decode x_1 and its own signal x_2. The coverage probability of $\mathcal{U}_2$ is expressed as

$$
\begin{aligned}
&\mathcal{P}_{2\to\text{near}}^{\text{HD-CUP}} \\
&\quad = \Pr\left(\gamma_{2,1}^{\text{H}} \geq \tau_1, \gamma_{2,2}^{\text{H}} \geq \tau_2 | d_2 < d_1\right) \\
&\quad \overset{(a)}{=} \mathbf{1}(a_f > \frac{\tau_1}{1+\tau_1})\int_{\frac{\pi}{2}}^{\frac{3\pi}{2}}\int_0^{\min\left\{-2d_1\cos\theta,-\frac{d_1}{\cos\theta}\right\}} \\
&\qquad \times e^{-\max\left\{\frac{\sigma^2\tau_1 d_2^\alpha}{P_a\left(a_f-a_n\tau_1\right)},\frac{\sigma^2\tau_2 d_2^\alpha}{a_n P_a}\right\}}\frac{\lambda_u r e^{-\pi\lambda_u r^2}}{\mathcal{P}_{1\to\text{far}}^{\text{CUP}}}drd\theta \\
&\quad = \mathbf{1}(a_f > \frac{\tau_1}{1+\tau_1})\int_{\frac{\pi}{2}}^{\frac{3\pi}{2}}\int_0^{\min\left\{-2d_1\cos\theta,-\frac{d_1}{\cos\theta}\right\}} \\
&\qquad \times e^{-A\left(r^2+d_1^2+2rd_1\cos\theta\right)^{\frac{\alpha}{2}}}\frac{\lambda_u r e^{-\pi\lambda_u r^2}}{\mathcal{P}_{1\to\text{far}}^{\text{CUP}}}drd\theta, \qquad (26)
\end{aligned}
$$

where the $\mathbf{1}(a_f > \frac{\tau_1}{1+\tau_1})$ term in (a) assures the feasibility of $\gamma_{2,1}^{\text{H}} - \tau_1 \geq 0$ and the outage event occurs at the near user if it is violated. (8) is approximated by employing $u = -\frac{r}{d_1\cos\theta} - 1$, $v = -2\sqrt{2}\cos\theta - 1$, $u = -\frac{2r\cos\theta}{d_1} - 1$, $v = \frac{-4\cos u - 2\sqrt{2}}{2-\sqrt{2}} - 1$ and Gaussian-Chebyshev quadrature.

The coverage probability of $\mathcal{U}_1$ is

$$
\begin{aligned}
&\mathcal{P}_{1\to\text{far}}^{\text{HD-CUP}} \\
&= \Pr\left(\gamma_{2,1}^{\text{H}} \geq \tau_1, \gamma_{1,1}^{\text{H}} \geq \tau_1 | d_2 < d_1\right) \\
&= \mathbf{1}(a_f > \frac{\tau_1}{1+\tau_1})\int_{\frac{\pi}{2}}^{\frac{3\pi}{2}}\int_0^{\min\left\{-2d_1\cos\theta,-\frac{d_1}{\cos\theta}\right\}}\int_0^{\infty} \\
&\quad \times e^{-\frac{\sigma^2\tau_1}{P_a\left(a_f-a_n\tau_1\right)}d_2^\alpha-\frac{\sigma^2 d_3^\alpha}{P_u}\left(\tau_1-\frac{a_f P_a h_1}{a_n P_a h_1+\sigma^2 d_1^\alpha}\right)-h_1}
\end{aligned}
$$

$$
\begin{aligned}
&\times \frac{\lambda_u r e^{-\pi\lambda_u r^2}}{\mathcal{P}_{1\to\text{far}}^{\text{CUP}}} dh_1 dr d\theta \\
&\overset{(b)}{>} \mathbf{1}\left(a_f > \frac{\tau_1}{1+\tau_1}\right) \int_{\frac{\pi}{2}}^{\frac{3\pi}{2}} \int_0^{\min\left\{-2d_1\cos\theta, -\frac{d_1}{\cos\theta}\right\}} \int_0^{\infty} \\
&\quad e^{-Cd_2^{\alpha} - Dr^{\alpha} - \frac{Er^{\alpha}}{h_1} - h_1} \frac{\lambda_u r e^{-\pi\lambda_u r^2}}{\mathcal{P}_{1\to\text{far}}^{\text{CUP}}} dh_1 dr d\theta \\
&\overset{(c)}{=} \mathbf{1}\left(a_f > \frac{\tau_1}{1+\tau_1}\right) \int_{\frac{\pi}{2}}^{\frac{3\pi}{2}} \int_0^{\min\left\{-2d_1\cos\theta, -\frac{d_1}{\cos\theta}\right\}} e^{-Cd_2^{\alpha} - Dr^{\alpha}} \\
&\quad \times PPP2\sqrt{Er^{\alpha}} K_1\left(2\sqrt{Er^{\alpha}}\right) \frac{\lambda_u r e^{-\pi\lambda_u r^2}}{\mathcal{P}_{1\to\text{far}}^{\text{CUP}}} dr d\theta \\
&\overset{(d)}{\approx} \mathbf{1}\left(a_f > \frac{\tau_1}{1+\tau_1}\right) \int_{\frac{\pi}{2}}^{\frac{3\pi}{2}} \int_0^{\min\left\{-2d_1\cos\theta, -\frac{d_1}{\cos\theta}\right\}} e^{-Cd_2^{\alpha} - Dr^{\alpha}} \\
&\quad \times \left(1 + 2Er^{\alpha}c_0 + Er^{\alpha}\ln\left(Er^{\alpha}\right)\right) \frac{\lambda_u r e^{-\pi\lambda_u r^2}}{\mathcal{P}_{1\to\text{far}}^{\text{CUP}}} dr d\theta,
\end{aligned} \tag{27}
$$

where (b) follows from $\frac{a_f P_a h_1}{a_n P_a h_1 + \sigma^2 d_1^{\alpha}} = \frac{a_f}{a_n} - \frac{\frac{a_f}{a_n}\sigma^2 d_1^{\alpha}}{a_n P_a h_1 + \sigma^2 d_1^{\alpha}} > \frac{a_f}{a_n} - \frac{a_f \sigma^2 d_1^{\alpha}}{a_n^2 P_a h_1}$, (c) is obtained by using [31, eq. (3.324)], $K_1(\cdot)$ is the modified Bessel function for the second kind, (d) is approximated with high SNR regime using the series representation of Bessel functions $xK_1(x) \approx 1 + \frac{x^2}{2}\left(\ln\frac{x}{2} + c_0\right)$ [31]. (9) is obtained by employing the same algebraic transformations as in (26).

APPENDIX C
PROOF OF THEOREM 2

When $\mathcal{U}_2$ is the far user, the integral region is divided into three parts to simplify the analysis. That is,

$$
\begin{aligned}
&\mathcal{P}_{2\to\text{far}}^{\text{HD-CUP}} \\
&= \Pr\left(\gamma_{1,2}^{\text{H}} \ge \tau_2, \gamma_{2,2}^{\text{H}} \ge \tau_2 | d_2 > d_1\right) \\
&> \mathbf{1}\left(a_f > \frac{\tau_1}{1+\tau_1}\right) \left(\underbrace{2\int_{\frac{\pi}{2}}^{\frac{3\pi}{4}} \int_{-2d_1\cos\theta}^{-\frac{d_1}{\cos\theta}} X(r,\theta) dr d\theta}_{\varphi_1} \right. \\
&\quad \left. + \underbrace{\int_{-\frac{\pi}{2}}^{\frac{\pi}{2}} \int_0^1 X(r,\theta) dr d\theta}_{\varphi_2} + \underbrace{\int_{-\frac{\pi}{2}}^{\frac{\pi}{2}} \int_1^{\infty} X(r,\theta) dr d\theta}_{\varphi_3} \right),
\end{aligned} \tag{28}
$$

where

$$
\begin{aligned}
X(r,\theta) = &\frac{e^{-J-Kr^{\alpha}} \lambda_u r e^{-\pi\lambda_u r^2}}{1 - \mathcal{P}_{1\to\text{far}}^{\text{CUP}}} \\
&\times \left(1 + Lr^{\alpha} d_2^{\alpha}\left(\ln\left(Lr^{\alpha} d_2^{\alpha}\right) + 2c_0\right)\right).
\end{aligned}
$$

The first term φ_1 in (28) is obtained with $u = \frac{2r + 4d_1\cos\theta}{-\frac{d_1}{\cos\theta} + 2d_1\cos\theta} - 1$, $v = -2\sqrt{2}\cos\theta - 1$. The second and third term in (28) can be approximated similarly.

APPENDIX D
PROOF OF THEOREM 4

When $\mathcal{U}_1$ is the far user, the average data rate of $\mathcal{U}_2$ is

$$
\begin{aligned}
&\mathcal{R}_{2\to\text{near}}^{\text{HD-CUP}} \\
&= \mathrm{E}\left[\frac{1}{2}\log_2(1 + \gamma_{2,2}^{\text{H}}) | d_2 < d_1, \gamma_{2,1}^{\text{H}} \ge \tau_1\right] \\
&\quad \times \Pr(\gamma_{2,1}^{\text{H}} \ge \tau_1 | d_2 < d_1) \\
&= \frac{\int_0^{\infty} \Pr\left(d_2 < d_1, \gamma_{2,1}^{\text{H}} \ge \tau_1, \frac{1}{2}\log_2(1 + \gamma_{2,2}^{\text{H}}) \ge y\right) dy}{\mathcal{P}_{1\to\text{far}}^{\text{CUP}}} \\
&= \int_0^{\infty} \frac{\Pr\left(d_2 < d_1, \gamma_{2,1}^{\text{H}} \ge \tau_1, \gamma_{2,2}^{\text{H}} \ge x\right)}{2\ln 2\,(x+1)\,\mathcal{P}_{1\to\text{far}}^{\text{CUP}}} dx \\
&\overset{(e)}{\approx} \mathbf{1}\left(a_f > \frac{\tau_1}{1+\tau_1}\right) \frac{2\pi^2}{MN} \sum_{m=1}^{M} \sum_{n=1}^{N} \sin\left(\frac{2m-1}{2M}\pi\right) \\
&\quad \times \sin\left(\frac{2n-1}{2N}\pi\right) \left[\Xi_{2\to\text{near}}^{\text{HD-CUP,RI}} \frac{\lambda_u \phi_1 \phi_3^2 d_1 e^{-\frac{\pi\lambda_u \phi_1^2 \phi_3^2}{2}}}{4\sqrt{2 - \phi_3{}^2}} \right. \\
&\quad \left. + \Xi_{2\to\text{near}}^{\text{HD-CUP,RII}} \frac{4(2-\sqrt{2})\lambda_u d_1 \phi_1 e^{-\frac{4\pi\lambda_u d_1^2}{(\phi_2 + 2\sqrt{2})^2}}}{\left((\phi_2 + 2\sqrt{2})^2\right)\sqrt{16 - (\phi_2 + 2\sqrt{2})^2}} \right],
\end{aligned} \tag{29}
$$

where (e) follows [31, eq. (3.352.2)].

REFERENCES

[1] S. M. R. Islam, N. Avazov, O. A. Dobre, and K.-S. Kwak, "Power-domain non-orthogonal multiple access (NOMA) in 5G systems: Potentials and challenges," *IEEE Commun. Surveys Tuts.*, vol. 19, no. 2, pp. 721–742, 2nd Quart., 2017.

[2] Q. Cui *et al.*, "Preserving reliability of heterogeneous ultra-dense distributed networks in unlicensed spectrum," *IEEE Commun. Mag.*, vol. 56, no. 6, pp. 72–78, Jun. 2018.

[3] Z. Ma, Z. Zhang, Z. Ding, P. Fan, and H. Li, "Key techniques for 5G wireless communications: Network architecture, physical layer, and MAC layer perspectives," *Sci. China Inf. Sci.*, vol. 58, no. 4, pp. 1–20, Apr. 2015.

[4] K. Higuchi and A. Benjebbour, "Non-orthogonal multiple access (NOMA) with successive interference cancellation for future radio access," *IEICE Trans. Commun.*, vol. 98, no. 3, pp. 403–414, 2015.

[5] X. Yue, Y. Liu, S. Kang, A. Nallanathan, and Z. Ding, "Outage performance of full/half-duplex user relaying in NOMA systems," in *Proc. IEEE ICC*, May 2017, pp. 1–6.

[6] X. Yue, Y. Liu, S. Kang, A. Nallanathan, and Z. Ding, "Exploiting full/half-duplex user relaying in NOMA systems," *IEEE Trans. Commun.*, vol. 66, no. 2, pp. 560–575, Feb. 2017.

[7] Z. Zhang, Z. Ma, M. Xiao, Z. Ding, and P. Fan, "Full-duplex device-to-device-aided cooperative nonorthogonal multiple access," *IEEE Trans. Veh. Technol.*, vol. 66, no. 5, pp. 4467–4471, May 2017.

[8] L. Zhang, J. Liu, M. Xiao, G. Wu, Y.-C. Liang, and S. Li, "Performance analysis and optimization in downlink NOMA systems with cooperative full-duplex relaying," *IEEE J. Sel. Areas Commun.*, vol. 35, no. 10, pp. 2398–2412, Oct. 2017.

[9] X. Li, C. Li, and Y. Jin, "Joint subcarrier pairing and power allocation for cooperative nonorthogonal multiple access," *IEEE Trans. Veh. Technol.*, vol. 66, no. 11, pp. 10577–10582, Nov. 2017.

[10] Z. Wei, X. Zhu, S. Sun, J. Wang, and L. Hanzo, "Energy-efficient full-duplex cooperative nonorthogonal multiple access," *IEEE Trans. Veh. Technol.*, vol. 67, no. 10, pp. 10123–10128, Oct. 2018.
[11] T. Do *et al.*, "Improving the performance of cell-edge users in NOMA systems using cooperative relaying," *IEEE Trans. Commun.*, vol. 66, no. 5, pp. 1883–1901, May 2018.
[12] G. Liu, X. Chen, Z. Ding, Z. Ma, and F. R. Yu, "Hybrid half-duplex/full-duplex cooperative non-orthogonal multiple access with transmit power adaptation," *IEEE Trans. Wireless Commun.*, vol. 17, no. 1, pp. 506–519, Jan. 2018.
[13] Y. Zhou, V. W. S. Wong, and R. Schober, "Dynamic decode-and-forward based cooperative NOMA with spatially random users," *IEEE Trans. Wireless Commun.*, vol. 17, no. 5, pp. 3340–3356, Mar. 2018.
[14] Y. Liu, Z. Ding, M. Elkashlan, and H. V. Poor, "Cooperative non-orthogonal multiple access with simultaneous wireless information and power transfer," *IEEE J. Sel. Areas Commun.*, vol. 34, no. 4, pp. 938–953, Apr. 2016.
[15] H. Wu, X. Tao, N. Zhang, D. Wang, S. Zhang, and X. Shen, "On base station coordination in cache- and energy harvesting-enabled HetNets: A stochastic geometry study," *IEEE Trans. Commun.*, vol. 66, no. 7, pp. 3079–3091, Jul. 2018.
[16] Z. Ding *et al.*, "Impact of user pairing on 5G nonorthogonal multiple-access downlink transmissions," *IEEE Trans. Veh. Technol.*, vol. 65, no. 8, pp. 6010–6023, Aug. 2016.
[17] M. B. Shahab, M. F. Kader, and S. Y. Shin, "A virtual user pairing scheme to optimally utilize the spectrum of unpaired users in non-orthogonal multiple access," *IEEE Signal Process. Lett.*, vol. 23, no. 12, pp. 1766–1770, Dec. 2016.
[18] M. B. Shahab and S. Y. Shin, "User pairing and power allocation for non-orthogonal multiple access: Capacity maximization under data reliability constraints," *Phys. Commun.*, vol. 30, pp. 132–144, Oct. 2018.
[19] W. Liang, Z. Ding, Y. Li, and L. Song, "User pairing for downlink non-orthogonal multiple access networks using matching algorithm," *IEEE Trans. Commun.*, vol. 65, no. 12, pp. 5319–5332, Dec. 2017.
[20] Z. Liu, L. Lei, N. Zhang, G. Kang, and S. Chatzinotas, "Joint beamforming and power optimization with iterative user clustering for MISO-NOMA systems," *IEEE Access*, vol. 5, pp. 6872–6884, 2017.
[21] Z. Zhang, H. Sun, and R. Q. Hu, "Downlink and uplink non-orthogonal multiple access in a dense wireless network," *IEEE J. Sel. Areas Commun.*, vol. 35, no. 12, pp. 2771–2784, Dec. 2017.
[22] M. B. Shahab and S. Y. Shin, "Time shared half/full-duplex cooperative noma with clustered cell edge users," *IEEE Commun. Lett.*, vol. 22, no. 9, pp. 1794–1797, Sep. 2018.
[23] D. Tse and P. Viswanath, *Fundamentals of Wireless Communication*. Cambridge, U.K.: Cambridge Univ. Press, 2005.
[24] S. Ikki and M. H. Ahmed, "Performance analysis of incremental relaying cooperative diversity networks over Rayleigh fading channels," *IET Commun.*, vol. 5, no. 3, pp. 337–349, Feb. 2011.
[25] Z. Bai, J. Jia, C.-X. Wang, and D. Yuan, "Performance analysis of SNR-based incremental hybrid decode-amplify-forward cooperative relaying protocol," *IEEE Trans. Commun.*, vol. 63, no. 6, pp. 2094–2106, Jun. 2015.
[26] S. Zhang, P. He, K. Suto, P. Yang, L. Zhao, and X. Shen, "Cooperative edge caching in user-centric clustered mobile networks," *IEEE Trans. Mobile Comput.*, vol. 17, no. 8, pp. 1791–1805, Aug. 2018.
[27] X. Liu, Y. Liu, X. Wang, and H. Lin, "Highly efficient 3-D resource allocation techniques in 5G for NOMA-enabled massive MIMO and relaying systems," *IEEE J. Sel. Areas Commun.*, vol. 35, no. 12, pp. 2785–2797, Dec. 2017.
[28] X. Sun *et al.*, "Joint beamforming and power allocation in downlink NOMA multiuser MIMO networks," *IEEE Trans. Wireless Commun.*, vol. 17, no. 8, pp. 5367–5381, Aug. 2018.
[29] Y. Yu, H. Chen, Y. Li, Z. Ding, L. Song, and B. Vucetic, "Antenna selection for MIMO nonorthogonal multiple access systems," *IEEE Trans. Veh. Technol.*, vol. 67, no. 4, pp. 3158–3171, Apr. 2018.
[30] F. B. Hildebrand, *Introduction to Numerical Analysis*. New York, NY, USA: Dover, 1987.
[31] I. S. Gradshteyn and I. M. Ryzhik, *Table of Integrals, Series and Products*, 6th ed. New York, NY, USA: Academic, 2000.
[32] A. H. Sakr and E. Hossain, "Analysis of K-tier uplink cellular networks with ambient RF energy harvesting," *IEEE J. Sel. Areas Commun.*, vol. 33, no. 10, pp. 2226–2238, Oct. 2015.
[33] J. Zhao, Y. Liu, K. K. Chai, Y. Chen, and M. Elkashlan, "Joint subchannel and power allocation for NOMA enhanced D2D communications," *IEEE Trans. Commun.*, vol. 65, no. 11, pp. 5081–5094, Nov. 2017.
[34] Z. Yan, S. Chen, Y. Ou, and H. Liu, "Energy efficiency analysis of cache-enabled two-tier HetNets under different spectrum deployment strategies," *IEEE Access*, vol. 5, pp. 6791–6800, 2017.

JIAZHEN ZHANG received the B.E. degree in communication engineering from the Beijing University of Posts and Telecommunications, Beijing, China, in 2015, where she is currently pursuing the Ph.D. degree in information and communication engineering. Her research interests are in the area of wireless communications, with current emphasis on the physical layer security and non-orthogonal multiple access.

XIAOFENG TAO (SM'13) received the B.S. degree in electrical engineering from Xi'an Jiaotong University, Xi'an, China, in 1993, and the M.S.E.E. and Ph.D. degrees in telecommunication engineering from the Beijing University of Posts and Telecommunications (BUPT), Beijing, China, in 1999 and 2002, respectively. He is currently a Professor with BUPT. He has authored or co-authored 250 papers and three books in wireless communication areas. He was an Inventor or a Co-Inventor of 74 patents. He currently focuses on 5G research. He is the Chair of the IEEE ComSoc Beijing Chapter.

HUICI WU received the B.S. degree in communication engineering from the Communication University of China, Beijing, China, in 2013, and the Ph.D. degree in information and communication engineering from the Beijing University of Posts and Telecommunications (BUPT), Beijing, in 2018. From 2016 to 2017, she was with the Broadband Communications Research Group, Department of Electrical and Computer Engineering, University of Waterloo, Waterloo, ON, Canada. She is currently an Assistant Professor with the School of Cyberspace Security, BUPT. Her research interests are in the area of wireless communications and networks, with current emphasis on the cooperation and physical layer security in air-to-ground integration networks.

XUEFEI ZHANG received the B.S. and Ph.D. degrees in telecommunications engineering from the Beijing University of Posts and Telecommunications (BUPT) in 2010 and 2015, respectively. From 2013 to 2014, she held a visiting position with the School of Electrical and Information Engineering, The University of Sydney, Australia. She is currently with the National Engineering Lab for Mobile Network Technologies, BUPT. Her research areas include mobile edge computing, data analysis, intelligent transportation system, and dynamic programming.